To the Graduate Council:

I am submitting herewith a thesis written by L. Brent Bates entitled "A Comparison of Measurements of Mean Velocity and Turbulence Intensity in an Unheated, Subsonic, Free-Jet Airflow Made Concurrently with a Laser Doppler Velocimeter and a Hot-Wire Anemometer." I have examined the final copy of this thesis for form and content and recommend that it be accepted in partial fulfillment of the requirements for the degree of Master of Science, with a major in Engineering Science.

James R. Maus

James R. Maus, Major Professor

We have read this thesis
and recommend its acceptance:

W. M. Farmer

Accepted for the Council:

The Graduate School

# A COMPARISON OF MEASUREMENTS OF MEAN VELOCITY AND TURBULENCE INTENSITY IN AN UNHEATED, SUBSONIC, FREE-JET AIRFLOW MADE CONCURRENTLY WITH A LASER DOPPLER VELOCIMETER AND A HOT-WIRE ANEMOMETER

A Thesis

Presented for the

Master of Science

Degree

The University of Tennessee, Knoxville

L. Brent Bates

August 1983

# ACKNOWLEDGEMENTS

A number of people have generously assisted me in the course of conducting this research and in the preparation of this thesis. I am indebted to Dr. James R. Maus, Dr. Mitsuru Kurosaka, and Dr. W. Michael Farmer, who served as my major professor and committee respectively. Special thanks go to Mr. James R. Goodman and to the members of the UTSI Gas Diagnostics Division, without whom the experimental results could not have been obtained. I also wish to thank two good friends, Fort and Elizabeth Gwinn, who supplied encouragement along the way.

And most importantly, I thank my wife, Ila, for her encouragement, assistance, and patience during the course of this work.

## ABSTRACT

A single-component, Bragg-diffracted laser Doppler velocimeter was used to measure the mean velocity and turbulence intensity in an unheated, subsonic, free-jet airflow. The results were compared to measurements taken concurrently with a hot-wire anemometer at axial positions 1, 2, 4, and 8 nozzle diameters downstream of the nozzle exit plane. Favorable agreement was obtained for the mean velocity results at all but one axial station. Significant anomalies were noted in the LDV results for turbulence intensity when compared to the hot-wire results. Several possible sources for the discrepancies were identified including broad confidence intervals in the LDV data due to the small sample size, LDV probe volume and hot-wire probe misalignment, differences in the components of velocity sensed by the two probes, low frequency oscillations in the airflow due to control problems, and LDV signal processor parameter selection.

# TABLE OF CONTENTS


| CHAPTER | | PAGE |
|---|---|---|
| I. | INTRODUCTION | 1 |
| II. | EXPERIMENTAL APPARATUS AND PROCEDURE | 6 |
| | Air Supply System | 6 |
| | Laser Doppler Velocimeter System | 6 |
| | Hot-wire Anemometer System | 13 |
| | Experimental Procedure | 15 |
| III. | RESULTS | 22 |
| | Mean Velocity Measurements | 27 |
| | Turbulence Intensity Measurements | 32 |
| IV. | DISCUSSION OF RESULTS | 38 |
| | Statistical Considerations | 47 |
| | Geometric Considerations | 55 |
| | Airflow Control Considerations | 58 |
| | Particle Dynamics Considerations | 59 |
| | Signal Processor Parameter Considerations | 60 |
| V. | CONCLUSIONS AND RECOMMENDATIONS | 63 |
| | Conclusions | 63 |
| | Recommendations | 64 |
| BIBLIOGRAPHY | | 66 |
| VITA | | 69 |

# LIST OF TABLES


| TABLE | | PAGE |
|---|---|---|
| I. | SUMMARY OF NOMINAL TEST CONDITIONS . . . . . | 23 |
| II. | LDV DATA ANALYSIS SUMMARY AT $X/D_e = 1$ . . . . . | 49 |
| III. | LDV DATA ANALYSIS SUMMARY AT $X/D_e = 2$ . . . . . | 50 |
| IV. | LDV DATA ANALYSIS SUMMARY AT $X/D_e = 4$ . . . . . | 51 |
| V. | LDV DATA ANALYSIS SUMMARY AT $X/D_e = 8$ . . . . . | 52 |

# LIST OF FIGURES


| FIGURE | | PAGE |
|---|---|---|
| 1. | LDV probe volume showing interference fringe formation | 3 |
| 2. | Schematic of air supply system | 7 |
| 3. | Dual-beam, forward scatter LDV optics configuration | 8 |
| 4. | LDV signal processor system | 10 |
| 5. | Doppler burst processor signals | 11 |
| 6. | Hot-wire anemometer signal processor system | 14 |
| 7. | Side view of test apparatus configuration | 16 |
| 8. | Top view of test apparatus configuration | 17 |
| 9. | Sample LDV calibration output | 18 |
| 10. | Sample LDV measurement printout | 26 |
| 11. | Mean axial velocity measurements at $x/D_e = 1$ | 28 |
| 12. | Mean axial velocity measurements at $x/D_e = 2$ | 29 |
| 13. | Mean axial velocity measurements at $x/D_e = 4$ | 30 |
| 14. | Mean axial velocity measurements at $x/D_e = 8$ | 31 |
| 15. | Turbulence intensity measurements at $x/D_e = 1$ | 33 |
| 16. | Turbulence intensity measurements at $x/D_e = 2$ | 34 |
| 17. | Turbulence intensity measurements at $x/D_e = 4$ | 35 |
| 18. | Turbulence intensity measurements at $x/D_e = 8$ | 36 |
| 19. | Comparison of LDV and hot-wire measurements of mean velocity at $x/D_e = 1$ | 39 |

FIGURE PAGE

20. Comparison of LDV and hot-wire measurements of mean velocity at $x/D_e = 2$ . . . . . 40

21. Comparison of LDV and hot-wire measurements of mean velocity at $x/D_e = 4$ . . . . . 41

22. Comparison of LDV and hot-wire measurements of mean velocity at $x/D_e = 8$ . . . . . 42

23. Comparison of LDV and hot-wire measurements of turbulence intensity at $x/D_e = 1$ . . . . . 43

24. Comparison of LDV and hot-wire measurements of turbulence intensity at $x/D_e = 2$ . . . . . 44

25. Comparison of LDV and hot-wire measurements of turbulence intensity at $x/D_e = 4$ . . . . . 45

26. Comparison of LDV and hot-wire measurements of turbulence intensity at $x/D_e = 8$ . . . . . 46

27. Confidence intervals for LDV mean velocity measurements at $x/D_e = 2$ . . . . . 53

28. Confidence intervals for LDV turbulence intensity measurements at $x/D_e = 2$ . . . . . 54

29. Comparison of LDV results using arithmetic and harmonic means . . . . . 56

30. Coordinate system for fluid flow . . . . . 57

31. Minimum acceptable velocity for various LDV high pass filter settings . . . . . 61

# NOMENCLATURE

| | |
|---|---|
| $D$ | Diameter, ft |
| $f_c$ | Clock frequency, MHz |
| $g_c$ | Proportionality constant, 32.174 ft-lbm/lbf-sec$^2$ |
| $M$ | Mach number; number of samples in a data set |
| $\dot{m}$ | Mass flow, lbm/sec |
| $N$ | Fringe counts |
| $n$ | Clock counts |
| $p_a$ | Ambient pressure, psfa |
| $p_o$ | Stilling chamber total pressure, psfa |
| $R$ | Gas constant, ft-lbf/lbm-$^oR$ |
| $R^2$ | Correlation coefficient |
| $R_{e_D}$ | Reynolds number based on nozzle exit diameter |
| $r$ | Radial position, ft |
| $T_o$ | Stilling chamber total temperature, $^oR$ |
| $TI$ | Turbulence intensity, $\sigma/Ue$ |
| $(TI)_\ell$ | Local turbulence intensity, $\sigma/\bar{U}$ |
| $Tol(TI)_\ell$ | Tolerance on local turbulence intensity |
| $Tol(\bar{U})$ | Tolerance on local mean velocity |
| $U$ | Axial velocity, ft/sec |
| $u$ | Fluctuating velocity component in x direction, ft/sec |
| $v$ | Fluctuating velocity component in y direction, ft/sec |

| | |
|---|---|
| w | Fluctuating velocity component in z direction, ft/sec |
| x | Axial position, ft; coordinate axis |
| y | Coordinate axis |
| Z | Confidence level |
| z | Coordinate axis |
| $\gamma$ | Ratio of specific heats |
| $\delta$ | Fringe spacing, $\mu$ft |
| $\epsilon$ | Signal aperiodicity |
| $\theta$ | Angle between centerlines of intersecting laser beams, degrees |
| $\kappa$ | Kurtosis |
| $\lambda$ | Wavelength, $\mu$ft |
| $\mu$ | Absolute viscosity, lbm/sec-ft |
| $\rho$ | Density, $lbm/ft^3$ |
| $\sigma$ | Standard deviation |
| $\tau$ | Time period, sec |

SUBSCRIPTS

| | |
|---|---|
| e | Nozzle exit |
| H-W | Hot-wire |
| i | Individual |
| L | Long counter set |
| LDV | Laser Doppler velocimeter |
| S | Short counter set |

SUPERSCRIPT

| | |
|---|---|
| $\bar{}$ | Mean value |

# CHAPTER I

## INTRODUCTION

Velocity measurements in turbulent fluid flows have, in the past, been made primarily with the hot-wire anemometer. Measurements with this device are based on determining the convective heat loss from an electrically heated wire caused by the flow of a gas or liquid surrounding the sensor (1)[1]. This device has the disadvantage that it disturbs the velocity at the measurement point, since a probe is physically inserted into the flow field. Additionally, the hot-wire is limited to low speed flows and moderate turbulence levels (2).

In recent years, the laser Doppler velocimeter (LDV) has been developed as an instrument for velocity measurements in turbulent flow fields (3,4,5,6,7,8). The LDV determines fluid flow velocity indirectly by measuring the Doppler shift of light scattered off of a moving particle in the fluid (9). The LDV is thus a noninterfering measurement device since only a laser beam is positioned in the flow field under study. The fluid must permit the laser light to penetrate it, and it must contain light-

---

[1]The numbers in parentheses refer to similarly numbered references in the bibliography.

scattering particles which are small enough to accurately follow the flow.

The basic concept of the operation of the LDV can be described by the interference fringe approach (3). In a dual scatter LDV system, two laser beams of equal intensity are caused to intersect, producing a region called the probe volume shown in Figure 1. The planar wavefronts of the beams intersect in this region, and, where the wavefronts are in phase, they reinforce each other to form a bright fringe. Where the wavefronts are 180 degrees out of phase they cancel each other, resulting in a dark region. The spacing between these fringes, $\delta$, is determined from

$$\delta = \frac{\lambda}{2 \sin(\theta/2)} \qquad (1)$$

where $\theta$ is the angle between the centerlines of the two intersecting beams, and $\lambda$ is the wavelength of the laser light.

A particle traversing the probe volume scatters light from the interference fringes which may be collected by a photomultiplier tube (PMT) and converted into an electrical signal of the form shown in Figure 1. The period of this signal, $\tau$, is the time required for the particle to travel a known distance, i.e., cross a known number of fringes, N, so the velocity of the particle, U, is determined by

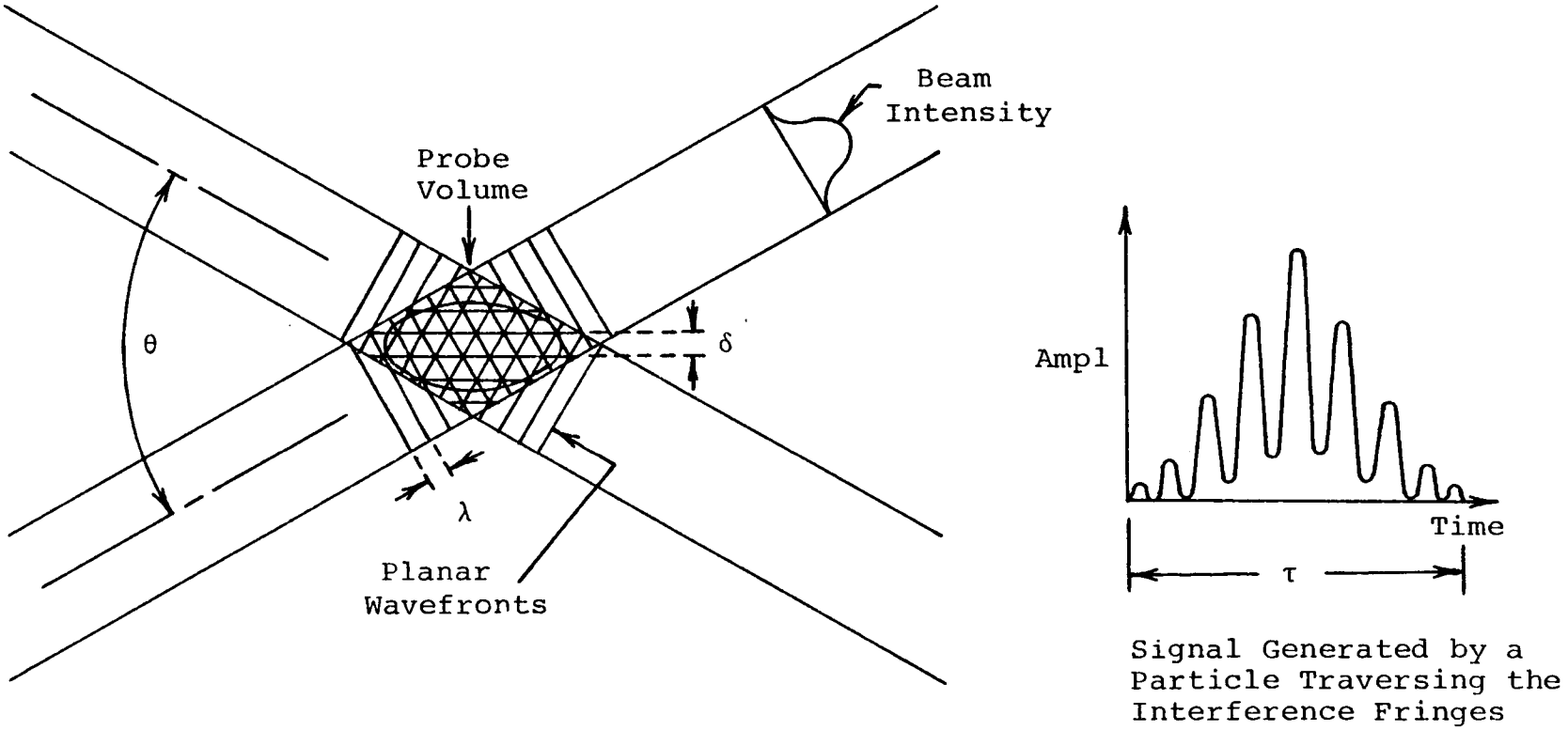



Figure 1. LDV probe volume showing interference fringe formation.

$$U = N \delta \frac{1}{\tau} \quad . \tag{2}$$

Several experimenters have investigated the performance of LDV systems applied to measuring turbulent flow field properties. Cline and Bentley (3) found that a large number of data points were required, particularly for the turbulence intensity measurements, to ensure a given accuracy and confidence level in the LDV results. Cliff, Fuller, and Sandborn (4) collected data from simultaneous measurements of turbulent gas fluctuations by a LDV and a hot-wire. Their results provide evidence that the LDV and hot-wire systems can measure the same instantaneous flow structures in a turbulent fluid flow. Barnett and Giel (5,6) have compared LDV and hot-wire measurements in subsonic jets. Comparisons of the results indicated anomalies in the turbulence intensity measurements for axial locations less than 10 nozzle diameters downstream. Several factors influencing the accuracy of the LDV results are discussed including optical alignment, statistical confidence and bias, particle dynamic behavior, and error characteristics of the LDV system. Giel (7) found no evidence of statistical bias in LDV results when compared to hot-wire and theoretical results. Flack (8) also identified several types of signal bias which may affect LDV measurements of mean velocity and turbulence intensity.

The present study was undertaken to compare mean velocity and turbulence intensity measurements obtained with an LDV system, developed by personnel in the Gas Diagnostics Division at UTSI, with measurement results obtained concurrently with a hot-wire anemometer. These measurements were made at several locations in an unheated, subsonic, free-jet airflow. It was desired to determine the suitability of the LDV for making measurements in turbulent flow fields for possible applications in aero-acoustic studies.

# CHAPTER II

# EXPERIMENTAL APPARATUS AND PROCEDURE

## Air Supply System

The tests were conducted using a free-jet test installation in the Aeroacoustics Laboratory at UTSI. A blow-down type air supply system was used to provide the desired airflows. This system is shown schematically in Figure 2. Air flowing from the high-pressure storage bottles was controlled by two globe regulators in series. The regulators were operated manually from a control panel in the laboratory. The unheated air entered a stilling chamber 10 inches in diameter and 44 inches long and emerged into still air from a circular nozzle 1.2 inches (3 cm) in diameter. A shielded iron-constantan thermocouple and a static pressure tap in the stilling chamber were used to monitor the total conditions of the airflow. Ambient pressure was measured with a recording barometer.

## Laser Doppler Velocimeter System

The LDV system used the dual-beam, forward scatter optical arrangement shown in Figure 3. A Spectra-Physics Model 171 argon ion laser, usually operated with an output power of 300 mW, provided a laser beam which was divided into two beams of equal intensity by a beam splitter, in

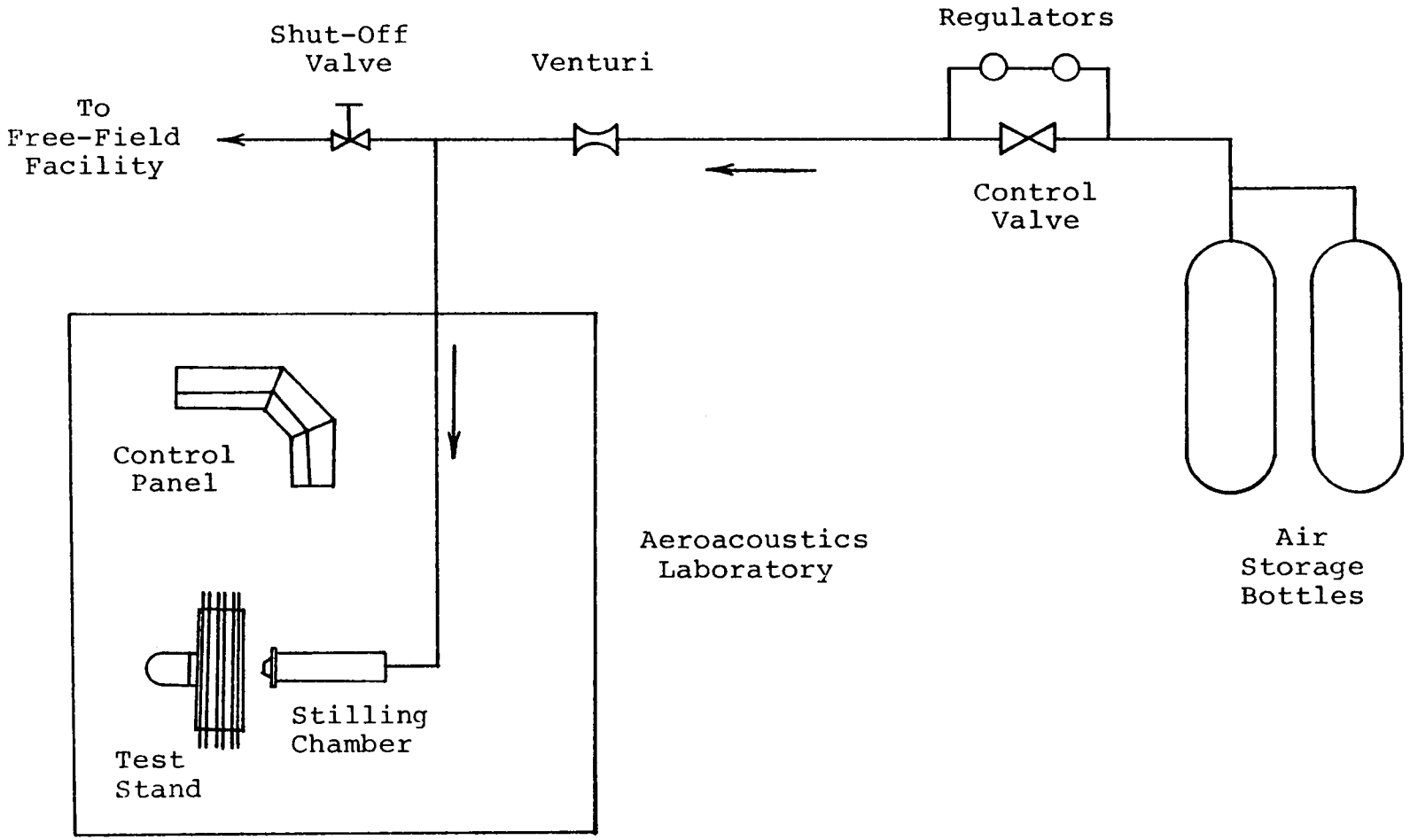



Figure 2. Schematic of air supply system.

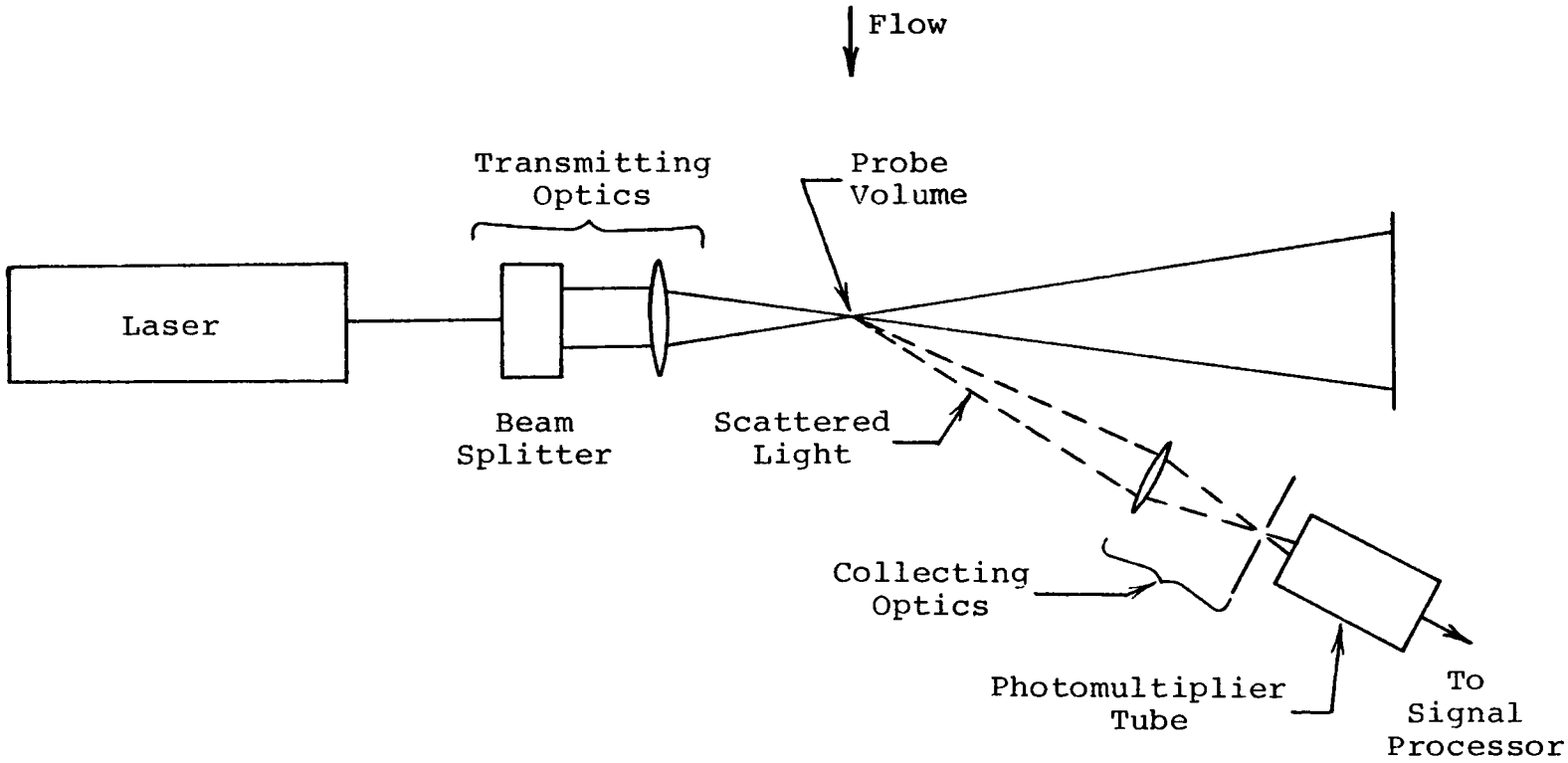



Figure 3. Dual-beam, forward scatter LDV optics configuration.

this case a Bragg diffraction cell. The two beams were then focused by lenses and caused to intersect, producing the probe volume. Light scattered from particles traversing this probe volume was collected and focused by lenses through an aperture into a photomultiplier tube (PMT). The output from the PMT was fed into the LDV signal processing system shown in Figure 4. This system was a digital burst processor consisting of a high pass filter, a zero-crossing detector, a clock, fringe and clock counters, a digital high pass filter, a Z-80 based microcomputer, a terminal for I/O, and a printer to obtain a hard copy of the measurement results. This signal processor was designed by Morris (10). Operating details pertinent to this study are discussed below.

The operation of the LDV burst processor is illustrated in Figure 5, which shows the conditioning a signal undergoes as it is processed by the system. At the top is the output signal from the PMT generated by a particle passing through the probe volume. Each peak corresponds to the particle crossing one of the interference fringes. The high pass filter removes the pedestal component from this signal leaving the Doppler component shown which enters the zero-crossing detector. This device generates a pulse for each peak in the filtered signal, producing the digital output shown. A preselected number, N, of these pulses are counted, and the time required to obtain

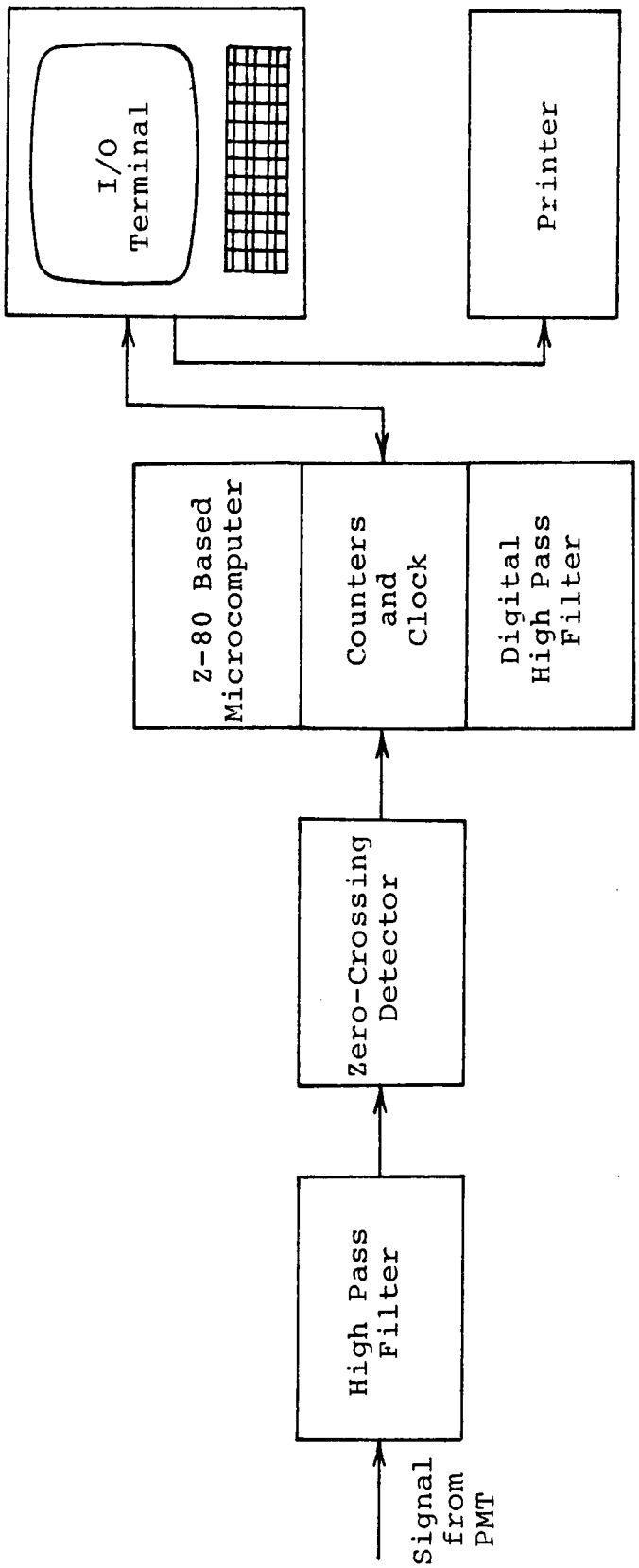



Figure 4. LDV signal processor system.

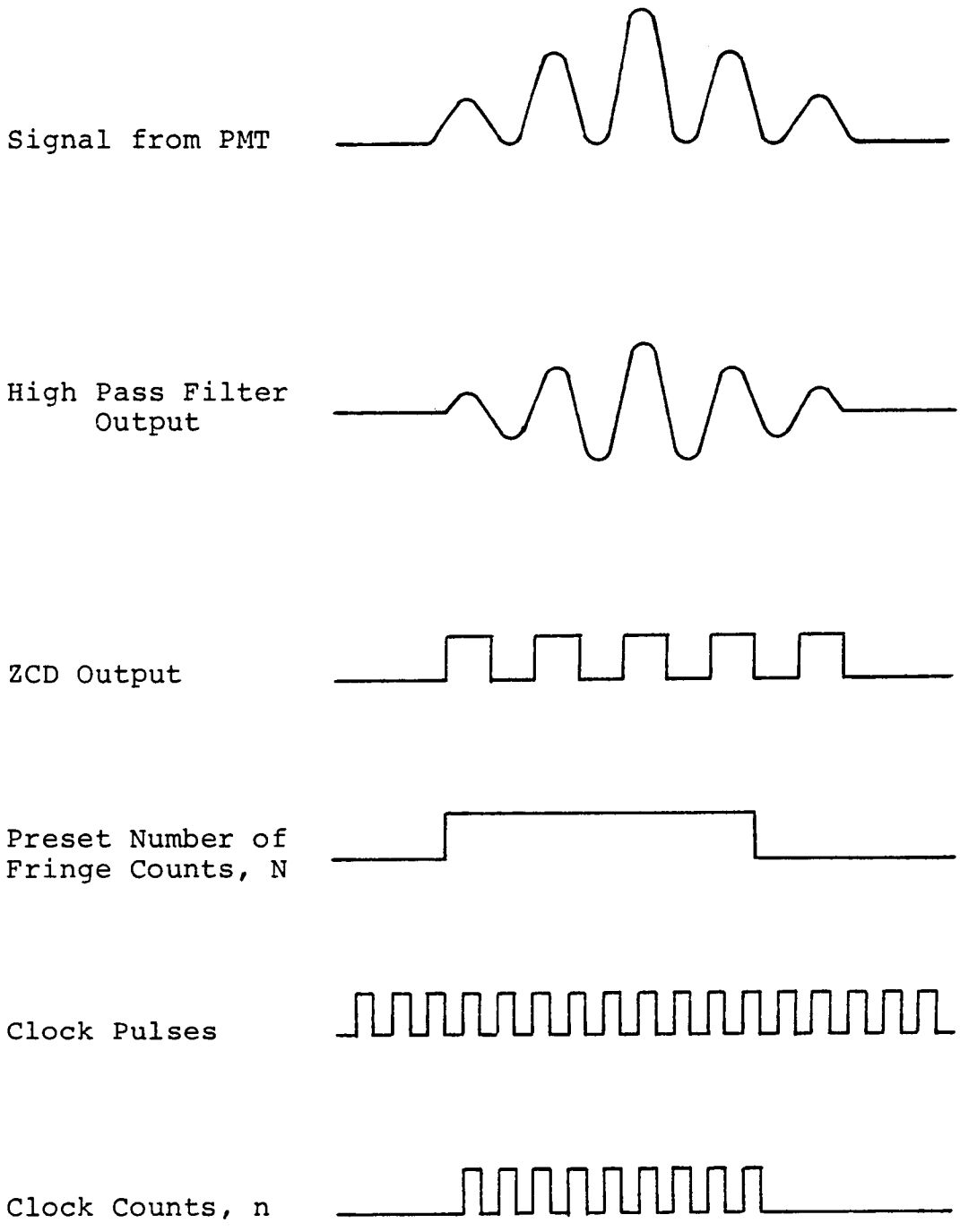



Figure 5. Doppler burst processor signals.

these pulses is determined. This time is found by counting the number of pulses, n, of a clock of known frequency, $f_c$, during the collection of N fringe counts. If the fringe spacing, $\delta$, is known, and this is determined by calibration, the velocity of the particle perpendicular to the interference fringes may be determined from

$$U = \frac{N \delta f_c}{n} \quad . \tag{3}$$

Also built into the LDV signal processor were a test for signal periodicity and a digital high pass filter. The test for periodicity was made in order to avoid errors caused by temporary dropout of the processor's input signal. This test was performed using two sets of fringe and clock counters, one LONG set and one SHORT set. The counts for each of these fringe and clock counters were used to determine the signal aperiodicity from

$$\varepsilon = \left| 1 - \frac{N_L n_S}{N_S n_L} \right| \quad . \tag{4}$$

If the signal aperiodicity exceeded a preset limit, that signal was rejected.

The digital high pass filter was used to avoid errors caused by large particles which tend to lag the airflow. The bias in the velocity determination caused by the relatively low velocity of these large particles could be reduced by selecting an appropriate frequency limit for this high pass filter. Additionally, a software high pass

filter test was built into the processor logic to detect any low frequency samples which may have eluded the digital high pass filter.

## Hot-Wire Anemometer System

The hot-wire probes used in this study were DISA Types 55A36 or 55A31. These probes have a platinum-plated tungsten wire 5 microns in diameter with an active length of approximately 1.25 mm. The hot-wire anemometer signal processing system is shown in Figure 6. The hot-wire probe was connected to a DISA Type 55D01 Constant Temperature Anemometer. The output from this device was linearized by a DISA Type 55D10 Linearizer. DC voltages, corresponding to mean velocity measurements, were displayed on a DISA Type 55D30 DC Voltmeter. A DISA Type 55D35 RMS Unit was used to display RMS voltages. A Honeywell SAI-42A Correlation and Probability Analyzer was used to provide a probability density function curve of the hot-wire anemometer output. These latter two units provided information regarding the turbulence of the flow. The output from the probability analyzer was viewed on a Tektronix, Inc. Type 515A Oscilloscope and recorded on a Technical Products Co. Model 135 X-Y Recorder. The oscilloscope and a DISA Type 55D25 Auxiliary Unit, which was used as a square wave generator, were utilized during calibration of the hot-wire anemometer system.

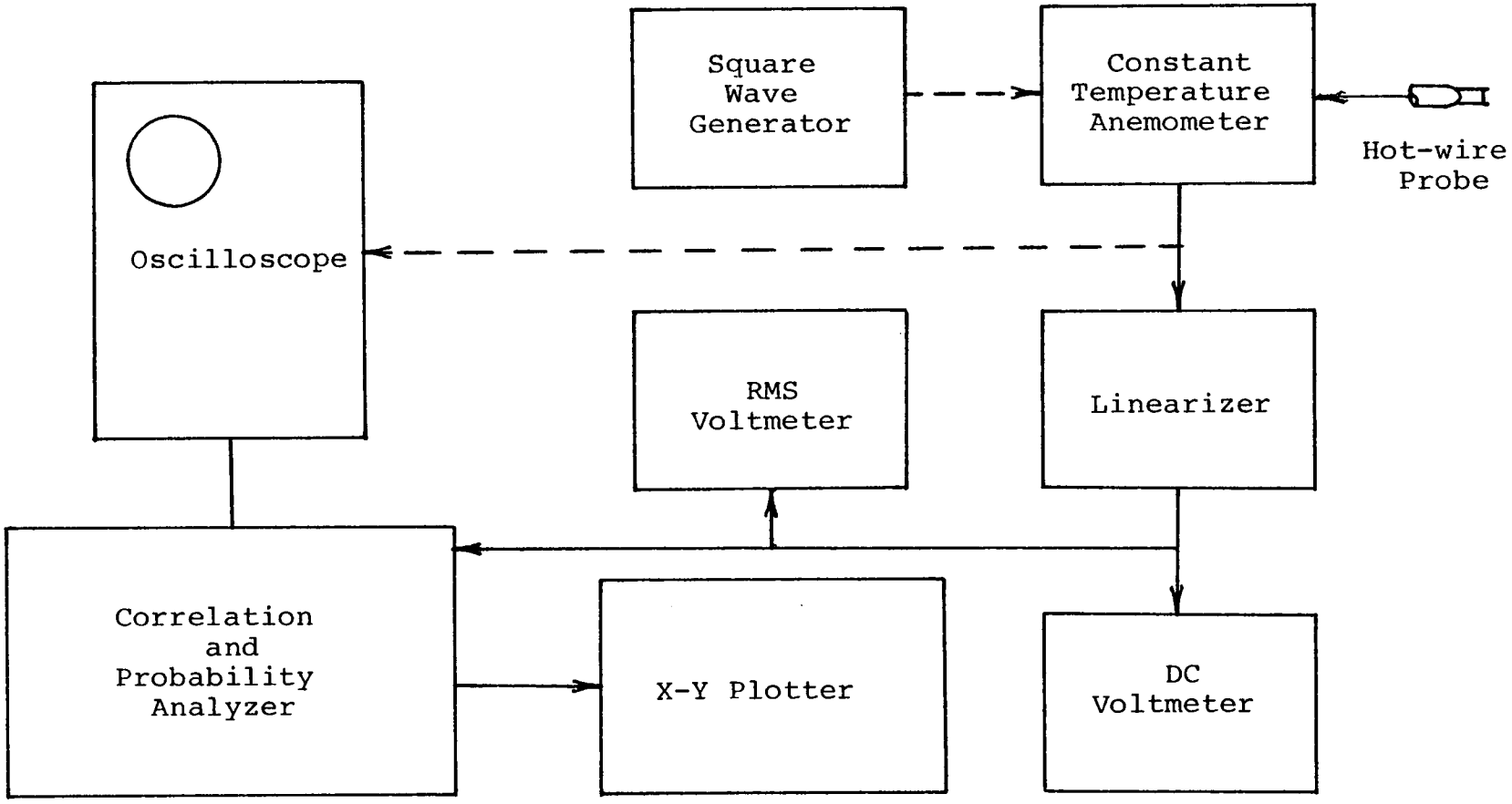



Figure 6. Hot-wire anemometer signal processor system.

## Experimental Procedure

The LDV optics and hot-wire probe were mounted on a rails attached to a plate which was fixed to a traversing bed. This arrangement was positioned in front of the free-jet nozzle as shown in Figures 7 and 8.

A typical test period began with the calibration of the LDV system. The optics were first aligned and then the system was calibrated with a small wire attached to the rim of a 4 inch diameter wheel rotating at 60 revolutions per second. This wheel was mounted so that the wire passed through the probe volume and intersected the interference fringes. The frequency of light scattered off the leading edge of this wire was used to determine the probe volume fringe spacing.

A typical computer printout of a rotating wheel calibration is shown in Figure 9. The LDV system operating parameters are listed at the top of the page. LONG COUNT and SHORT COUNT are the number of fringe counts required for each data sample. PRECOUNT is the number of fringe counts required before the LONG and SHORT counters are activated. This was used to ignore the first few counts when the signal-to-noise ratio is low. The CLOCK FREQUENCY and digital HIGH PASS FILTER frequency are shown in MHz. The FRINGE PERIOD was not used during calibration since this is the parameter being determined. During velocity

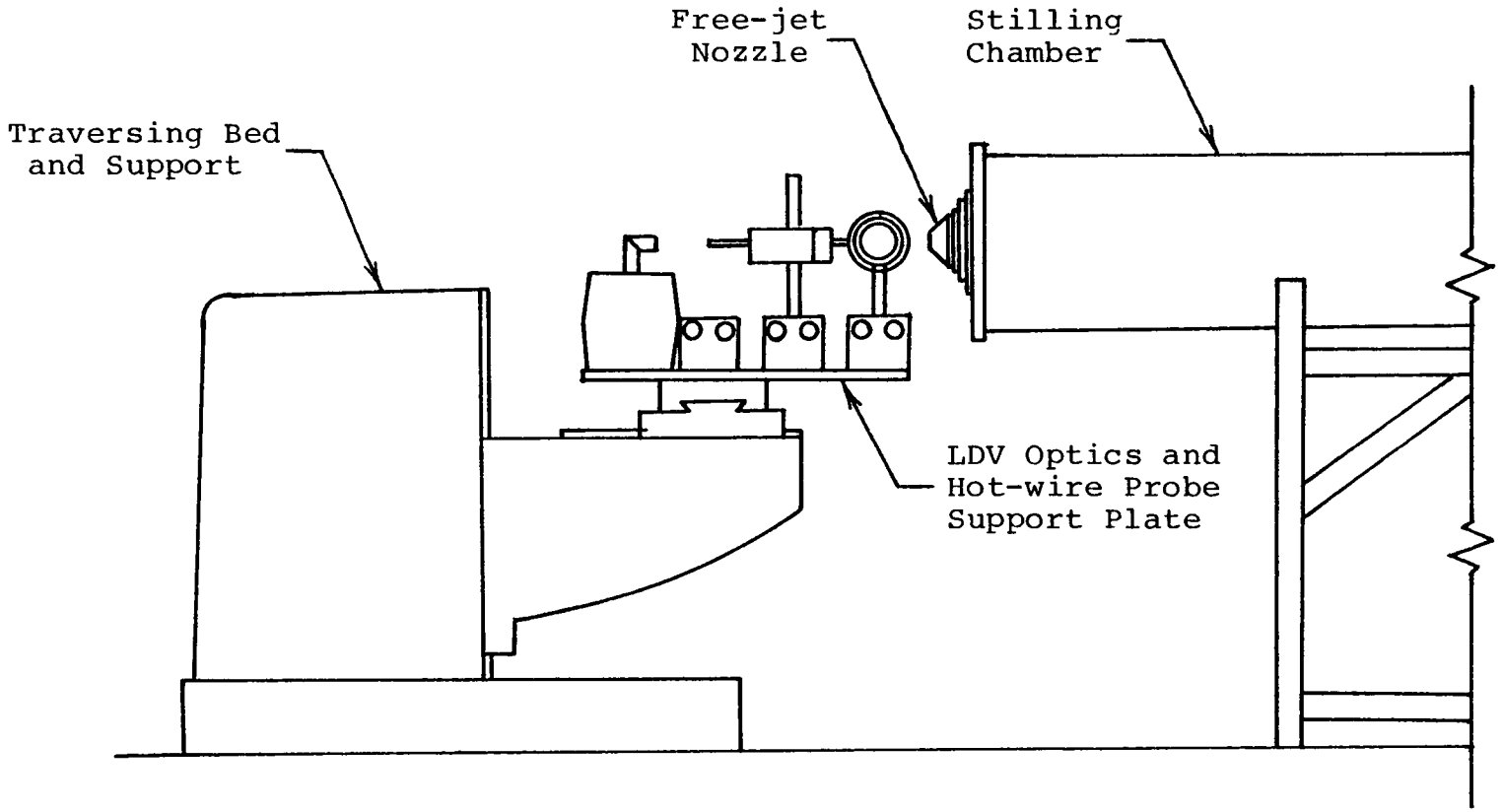



Figure 7. Side view of test apparatus configuration.

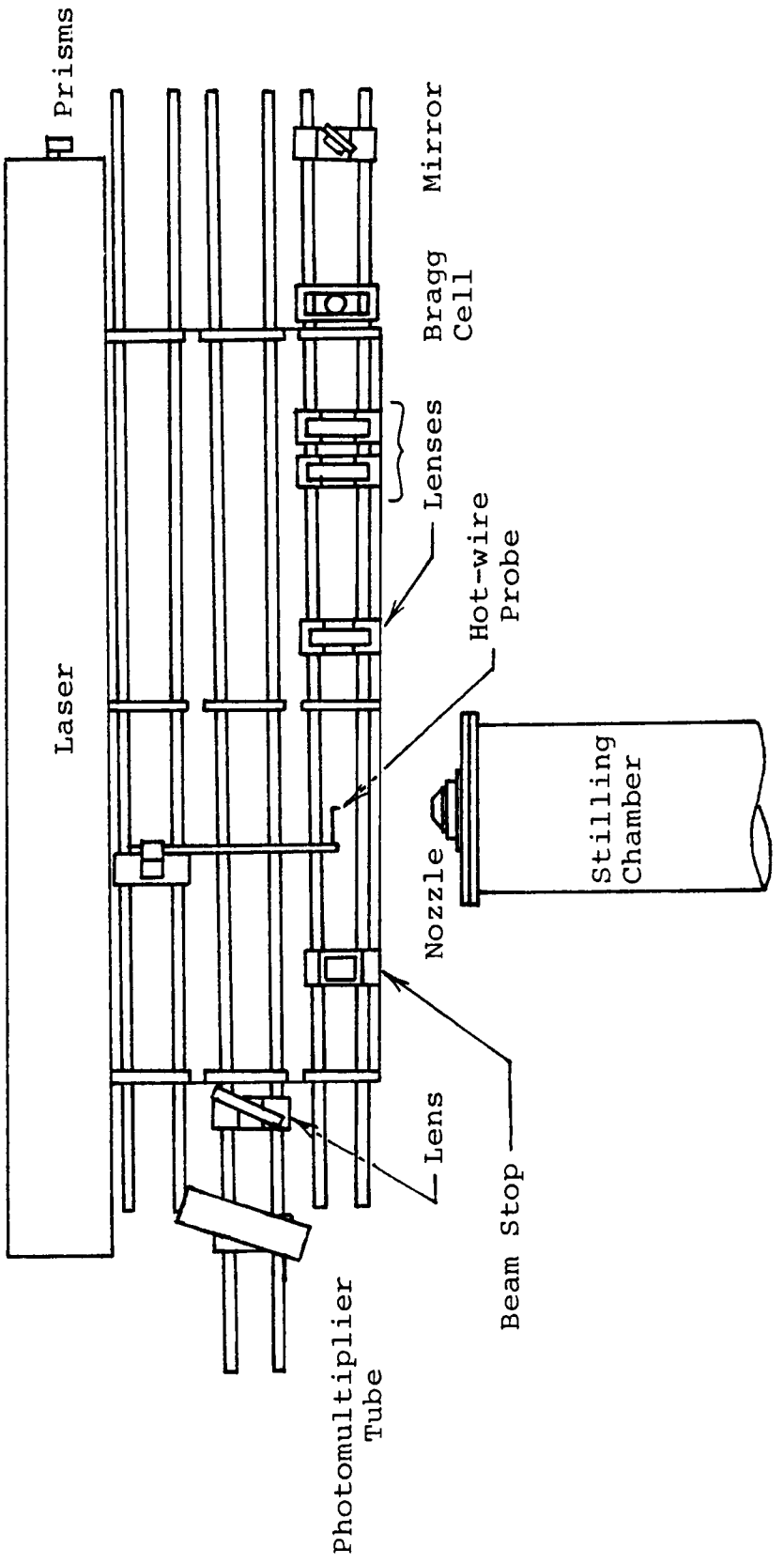



Figure 8. Top view of test apparatus configuration.

```
  U T S I   G A S   D I G N O S T I C S   D I V I S I O N
LONG COUNT              16
SHORT COUNT             9
PRECOUNT                3
CLOCK FREQUENCY         70.00
HIGH PASS FILTER        .9000
FRINGE PERIOD           1.000
MAX APERIODICITY        5.000
BIAS FREQUENCY          0.000
TIMER RATE              1000
SAMPLE SIZE             100
RUN NUMBER              47
DATE                      10-12-78  HOT-WIRE ANEMOMETER AND LDV COMPARISON
                        FREQUENCY MODE
                        GLOBAL =  10
                   ROTATING WHEEL CALIBRATION DATA
 FREQ      SIGNA          %        KAPPA       TAU      AFAIL   HPFAIL

 1.241     2.301E-03  .1853      2.268       .8052
 1.242     2.447E-03  .1970      3.377       .8050
 1.242     2.879E-03  .2318      5.079       .8051
 1.242     2.553E-03  .2055      3.170       .8050
 1.241     2.736E-03  .2203      8.612       .8051
 1.241     3.006E-03  .2421      6.248       .8052
 1.242     3.102E-03  .2497      3.115       .8049      1
 1.242     3.387E-03  .2725      3.722       .8045
 1.243     3.830E-03  .3121      11.19       .8043
 1.243     3.185E-03  .2562      2.777       .8044



AVERAGES (EXCEPT AFAIL AND HPFAIL)
 1.242     2.948E-03  .2372      4.056       .8049      1
```

Figure 9. Sample LDV calibration output.

measurements the value of the fringe spacing is listed in μft. MAX APERIODICITY is the upper limit in percent for the aperiodicity test discussed previously. BIAS FREQUENCY is the apparent frequency at which the interference fringes are moving. A value of 0 here indicates that the 15 MHz frequency shift in the laser light imparted by the Bragg cell has been removed, so that the signal being processed appears the same as it would if the fringes were stationary. TIMER RATE is the accuracy of a timer used to measure the elapsed time after the processor was reset until a particle generated a signal. A value of 1000 for this parameter indicates that the timer was accurate to the nearest msec. This time was not recorded during testing. SAMPLE SIZE, RUN NUMBER, and test DATE are also listed. GLOBAL = 10 indicates that 10 sets of samples were collected and averaged to produce the final results shown at the bottom of the printout under AVERAGES. Near the center of the printout the values listed under FREQ are the mean frequencies in MHz for each set of 100 samples. The SIGMA column lists the standard deviations in MHz, while the % column expresses these as percentages of the mean frequencies . The kurtosis for each set of measurements is given under the KAPPA heading. TAU lists the mean time periods in μsec. AFAIL and HFAIL list the number of samples which were rejected due to failing the aperiodicity and software high pass filter tests respectively.

Once the LDV system was calibrated, the hot-wire probe was aligned as well as possible with the LDV probe volume. The hot-wire was positioned approximately 1 MM downstream of and parallel to the probe volume. The laser power was then reduced as a safety precaution so that the hot-wire anemometer system could be calibrated.

The hot-wire probe was aligned with the free-jet nozzle centerline as close to the nozzle exit plane as possible. This position was noted by taking readings from the adjusting wheels on the traversing bed, and the probe was moved out of the flow region.

The desired airflow was then established. Stilling chamber pressure was adjusted to produce a nominal nozzle exit velocity of 300 ft/sec based on isentropic flow calculations, assuming the jet expands to ambient pressure at the nozzle exit.

The hot-wire probe was moved back to the nozzle centerline position, and the system was calibrated according to the procedures in Reference 1 and adjusted to give a DC voltage reading of 9 volts at the nominal exit velocity of 300 ft/sec.

The laser power was increased to the normal value, and the probe combination was moved to the desired position. The hot-wire data were recorded, a set of LDV measurements were taken, and a printout of the data was generated. The probe combination was moved to the next position and data

collected once again. This procedure was repeated until the desired number of test points had been run.

# CHAPTER III

## RESULTS

LDV and hot-wire measurements of mean velocity and turbulance intensity are presented. These data were obtained for radial cross-sections of the free-jet flow field at 1, 2, 4, and 8 nozzle diameters downstream of the nozzle exit plane. The nominal test conditions for each of these axial stations are presented in Table I. These parameters were calculated from the following formulas:

$$U_e = \sqrt{\frac{2\ \gamma\ R\ g_c}{\gamma - 1}\ T_o \left[1 - \left(\frac{p_a}{p_o}\right)^{\frac{\gamma - 1}{\gamma}}\right]} \tag{5}$$

$$M_e = \sqrt{\frac{2}{\gamma - 1}\left[\left(\frac{p_a}{p_o}\right)^{\frac{1 - \gamma}{\gamma}} - 1\right]} \tag{6}$$

$$\mu_e = \frac{(2.27 \times 10^{-8})\left[T_o\left(\frac{p_a}{p_o}\right)^{\frac{\gamma - 1}{\gamma}}\right]^{\frac{3}{2}}\ g_c}{T_o\left(\frac{p_a}{p_o}\right)^{\frac{\gamma - 1}{\gamma}} + 199} \tag{7}$$

$$\rho_e = \frac{p_a}{R\ T_o\left(\frac{p_a}{p_o}\right)^{\frac{\gamma - 1}{\gamma}}} \tag{8}$$

TABLE I

SUMMARY OF NOMINAL TEST CONDITIONS

| Axial Station, $X/D_e$ | Ambient Pressure, $P_a$ (psfa) | Stilling Chamber Pressure, $P_o$ (psfa) | Stilling Chamber Air Temp. $T_o$ ($^oR$) | Nozzle Exit Velocity, $U_e$ (ft/sec) | Nozzle Exit Mach No., $M_e$ | Nozzle Exit Reynolds No., $R_{e_D}$ | Mass Flow, $\dot{m}$ (lbm/sec) |
|---|---|---|---|---|---|---|---|
| 1 | 2051 | 2157 | 525 | 300 ± 9 | 0.269 | $1.86 \times 10^5$ | 0.175 |
| 2 | 2056 | 2161 | 533 | 301 ± 9 | 0.267 | $1.82 \times 10^5$ | 0.173 |
| 4 | 2069 | 2175 | 525 | 299 ± 9 | 0.268 | $1.87 \times 10^5$ | 0.176 |
| 8 | 2065 | 2172 | 520 | 299 ± 9 | 0.269 | $1.90 \times 10^5$ | 0.177 |

$$R_{e_D} = \frac{\rho_e U_e D_e}{\mu_e} \tag{9}$$

$$\dot{m} = \frac{\rho_e U_e \pi D_e^2}{4} \tag{10}$$

using the constants:

$$\gamma = 1.402$$

$$R = 53.35 \text{ ft-lbf/lbm-}^{\circ}R$$

$$g_c = 32.174 \text{ ft-lbm/lbf-sec}^2$$

$$D_e = 0.1 \text{ ft}$$

where $U_e$ is the nozzle exit velocity; $M_e$ is the nozzle exit Mach number; $\mu_e$ is the airflow absolute viscosity at the nozzle exit; $\rho_e$ is the density at the nozzle exit; $R_{e_D}$ is the Reynold's number based on $D_e$, the nozzle exit diameter; $\dot{m}$ is the mass flow rate; $\gamma$ is the ratio of specific heats; R is the gas constant for the airflow; $g_c$ is a proportionality constant; $T_o$ is the stilling chamber air total temperature; $p_o$ is the stilling chamber total pressure; and $p_a$ is the ambient pressure.

Also shown on Table I under the $U_e$ column is the estimated uncertainty for the calculated nozzle exit velocity. This estimate was determined by expanding Equation (5) in a Taylor series in $p_a$, $p_o$, and $T_o$ and evaluating the result at the maximum uncertainty for each parameter (11). This analysis yielded an uncertainty of approximately 3 percent at the nominal exit velocity of 300 ft/sec.

A printout of the LDV measurements at one station is shown in Figure 10. The parameters listed are the same as those in Figure 9, page 18, with the exception that the FREQ column has been replaced in Figure 10 by VEL. Under this column is the average velocity in ft/sec for each set of samples. The standard deviation, SIGMA, is now also shown in the units of ft/sec. Below the AVERAGES data are listed the individual velocities for the last set of samples collected at that station.

Note from Equation (3) that the calculated velocity is dependent upon 1/n, where n is the number of clock pulses counted during the collection of N fringe counts. The arithmetic average of the individual values of n is calculated by the processor for a given sample set, and this average is used to determine the mean velocity. This may be seen to be equivalent to taking the harmonic mean of the individual velocity values (12). The arithmetic mean of n is determined from

$$\bar{n} = \frac{1}{M} \sum_{i=1}^{M} n_i \quad . \tag{11}$$

The mean velocity is given by

$$\bar{U} = \frac{N \delta f_c}{\bar{n}} \quad . \tag{12}$$

Combining Equations (11) and (12) yields

```
   U T S I   G A S   D I G N O S T I C S   D I V I S I O N
LONG COUNT              16
SHORT COUNT             9
PRECOUNT                3
CLOCK FREQUENCY         70.00
HIGH PASS FILTER        5.000       208.0
FRINGE PERIOD           53.12
MAX APERIODICITY        5.000
BIAS FREQUENCY          0.000
TIMER RATE              1000
SAMPLE SIZE             100
RUN NUMBER              115
DATE                      10-12-78  HOT-WIRE ANEMOMETER AND LDV COMPARISON
                        VELOCITY MODE
                        GLOBAL =  10
TEST POINT #4
 VEL        SIGMA          %          KAPPA         TAU       AFAIL     HPFAIL
 295.1      24.36       8.254         5.895        .1000        53         17
 293.8      18.65       6.349         1.994        .1807        61          6
 296.7      18.56       6.256         2.063        .1790        56         15
 292.0      18.37       6.291         1.303        .1818        53         13
 292.8      19.94       6.811         2.261        .1813        53         11
 296.4      24.69       8.328         2.598        .1791        57         15
 290.8      20.35       6.996         2.693        .1826        55         13
 293.1      22.79       7.776         4.779        .1812        54          8
 291.4      20.97       7.197         1.833        .1822        59         10
 294.3      26.88       9.135         2.147        .1804        58          9



AVERAGES (EXCEPT AFAIL AND HPFAIL)
 293.6      21.56       7.339         2.807        .1808       559        117

 283.3
 283.3
 295.9      270.4
 321.5      283.3       286.0
 270.4      352.0

 286.0
 266.7      283.3       336.1         265.6
 287.4      330.5

 360.5      308.2       293.0
 284.6
 271.6      354.1
 270.4      332.3       275.4         291.6       278.0
 280.6      283.3       356.2
 265.6      318.1
 272.9
```

Figure 10. Sample LDV measurement printout.

$$\overline{U} = \frac{N \delta f_c}{\frac{1}{M} \sum_{i=1}^{M} n_i} \quad . \tag{13}$$

The individual velocity values are given by

$$U_i = \frac{N \delta f_c}{n_i} \quad . \tag{14}$$

Inverting both sides of Equation (14) and performing a summation on i yields

$$\sum_{i=1}^{M} \frac{1}{U_i} = \frac{\sum_{i=1}^{M} n_i}{N \delta f_c} \quad . \tag{15}$$

Combining Equations (13) and (15) results in

$$\overline{U} = \frac{M}{\sum_{i=1}^{M} \frac{1}{U_i}} \tag{16}$$

which is the harmonic mean velocity. In the above equations M is the number of individual samples in a given set.

## Mean Velocity Measurements

The radial distribution of axial velocity measured by the LDV and hot-wire systems at stations 1, 2, 4, and 8 nozzle diameters downstream of the nozzle exit plane are presented in Figures 11, 12, 13, and 14, respectively. The results have been normalized with respect to the nominal nozzle exit velocity, $U_e$. The radial position, r, has been normalized with respect to the nozzle exit radius,

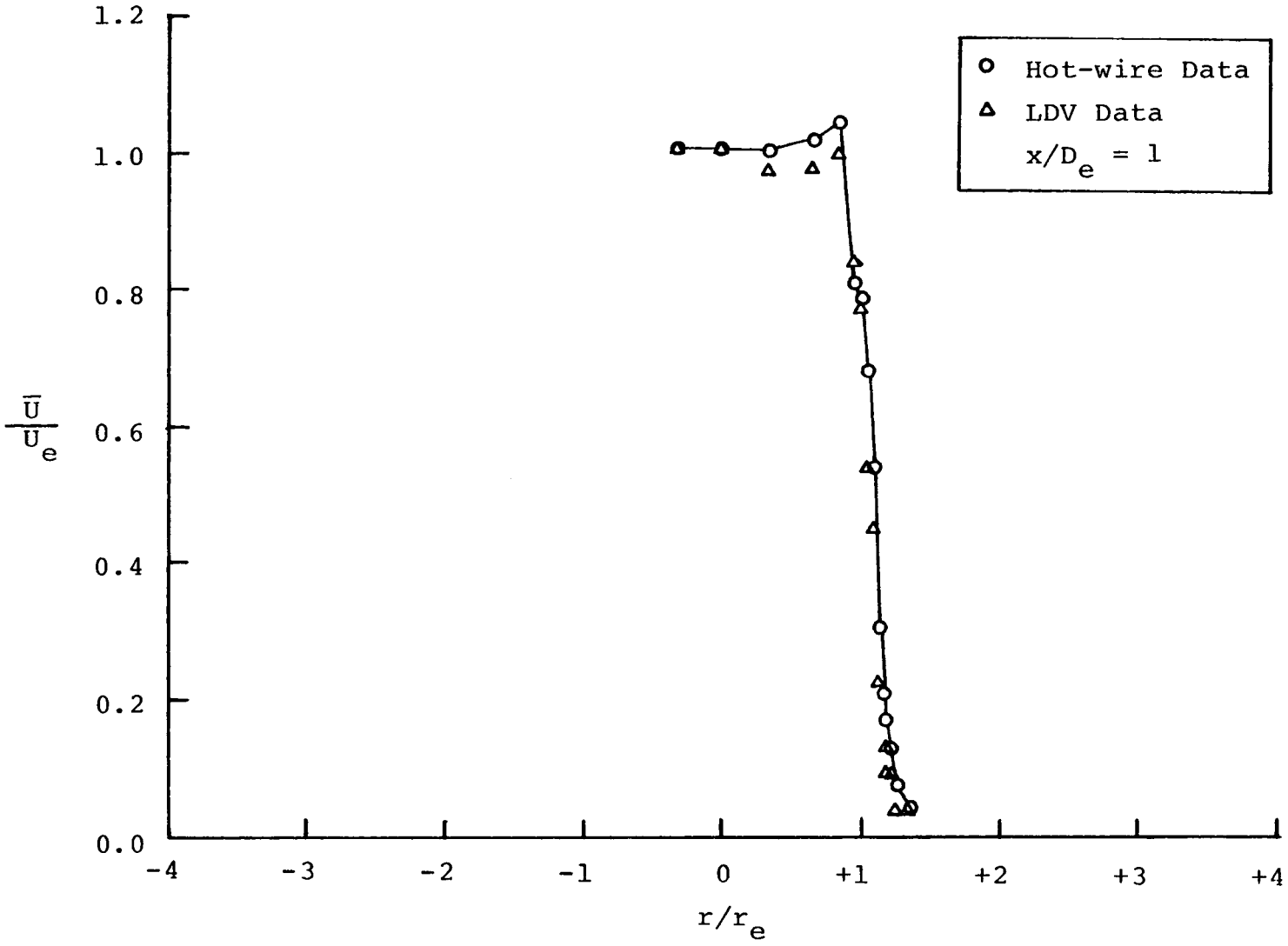



Figure 11. Mean axial velocity measurements at $x/D_e = 1$.

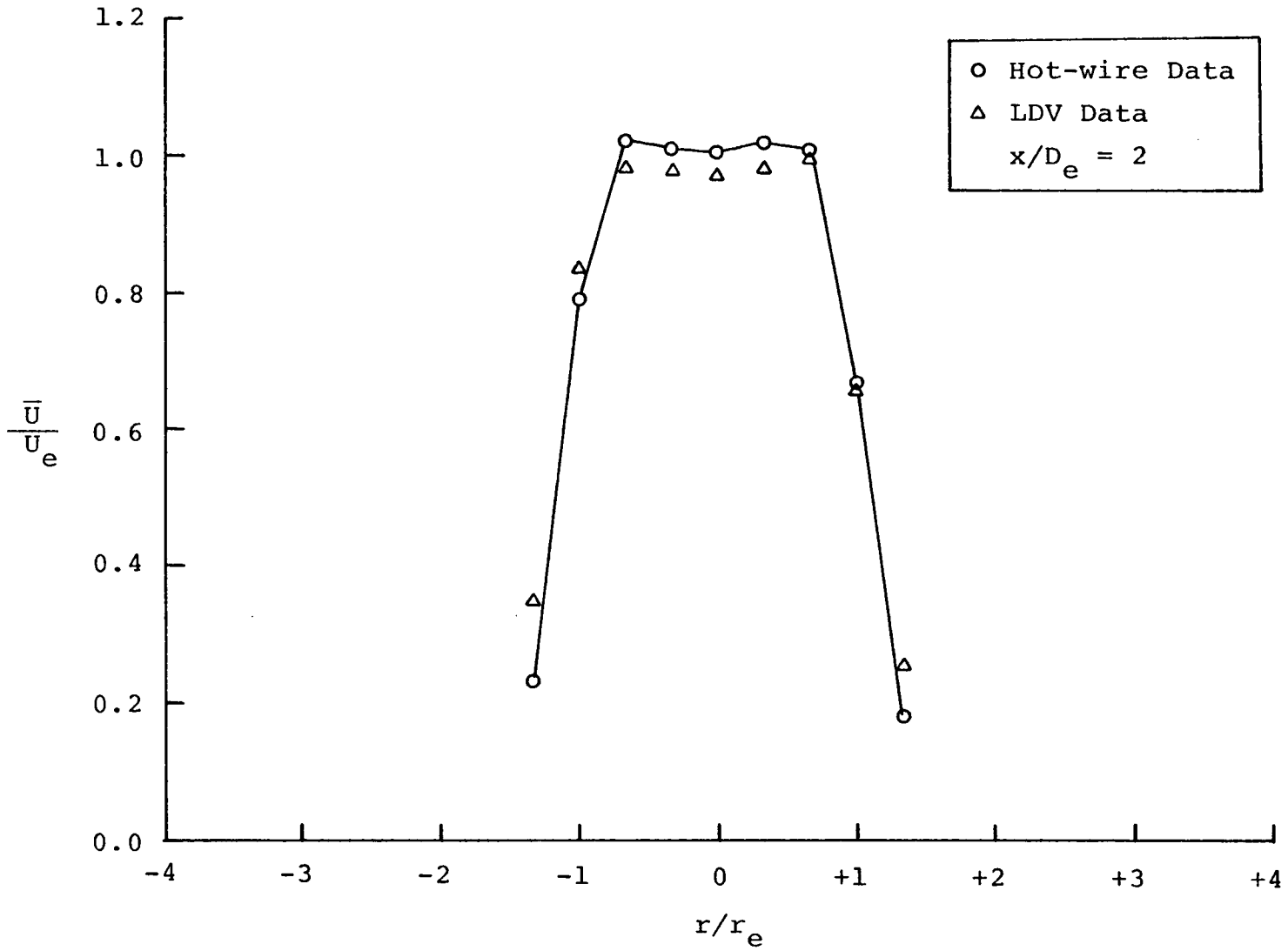



Figure 12. Mean axial velocity measurements at $x/D_e = 2$.

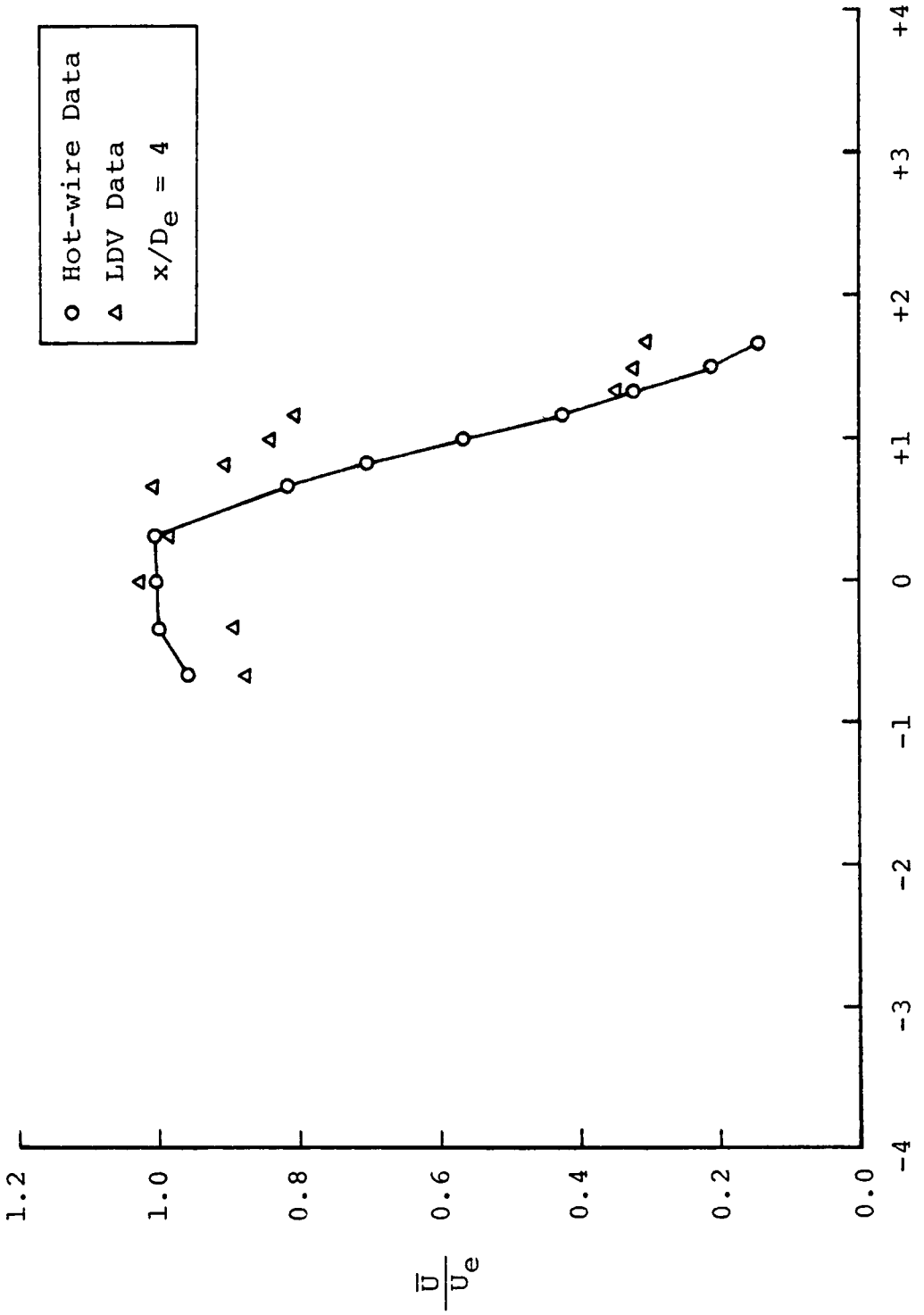



Figure 13. Mean axial velocity measurements at $x/D_e = 4$.

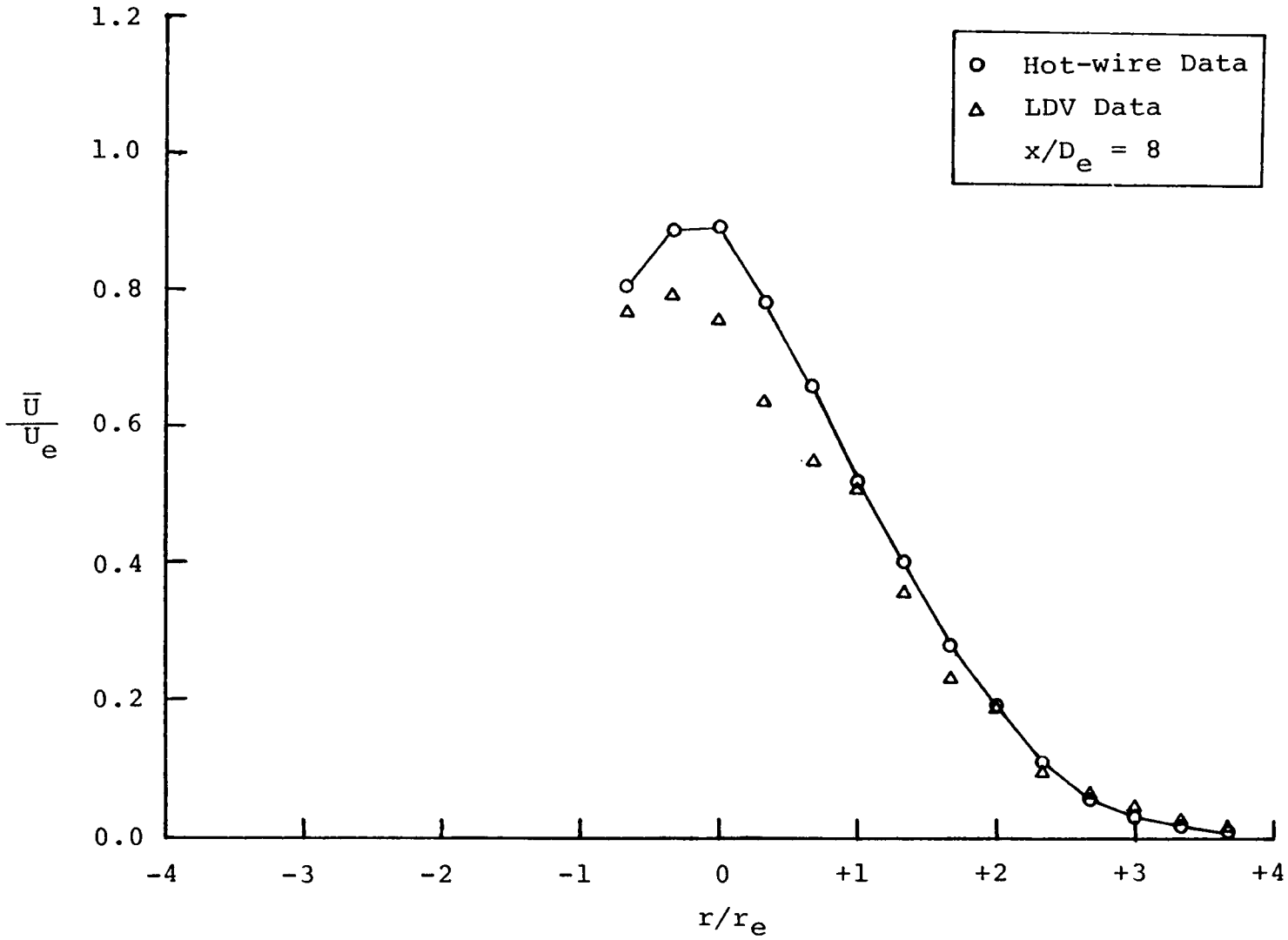



Figure 14. Mean axial velocity measurements at $x/D_e$ = 8.

$r_e$. A value of 0 for $r/r_e$ corresponds to the centerline of the jet.

It may be seen in Figures 11 and 12 that for $x/D_e$ = 1 and 2, respectively, the LDV and hot-wire results agree reasonably well. The velocities measured by the LDV near the center of the jet are lower than those for the hot-wire. This same trend is seen in Figure 14 for $x/D_e$ = 8, however the difference in centerline velocities is even more pronounced at this station. At $x/D_e$= 4, Figure 13, the LDV data show considerable scatter about the hot-wire results.

## Turbulence Intensity Measurements

The radial distribution of turbulence intensity as measured by the LDV and hot-wire systems for $x/D_e$ values of 1, 2, 4, and 8 are shown in Figures 15, 16, 17, and 18, respectively. The parameter TI is the standard deviation, $\sigma$, (i.e., the RMS value of the fluctuating velocity component) normalized with respect to the nominal jet exit velocity, $U_e$. The radial position is the same as that described previously for the mean velocity results.

At $x/D_e$ = 1 and 2, Figures 15 and 16, respectively, the LDV turbulence intensity measurements are seen to be greater than those for the hot-wire in both the jet centermine region and in the jet mixing region. At $x/D_e$ = 4 and 8, Figures 17 and 18, respectively, the centerline

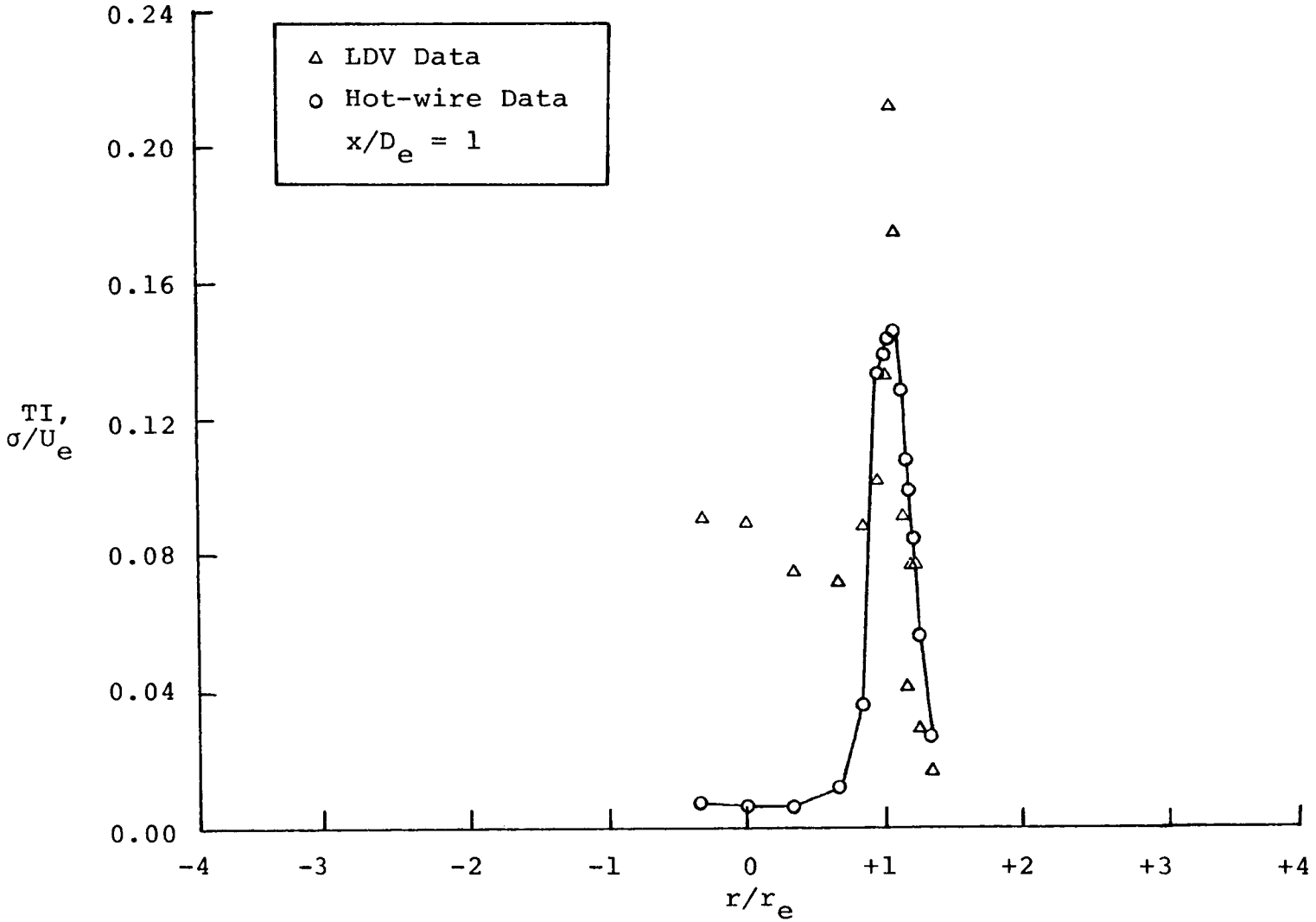



Figure 15. Turbulence intensity measurements at $x/D_e = 1$.

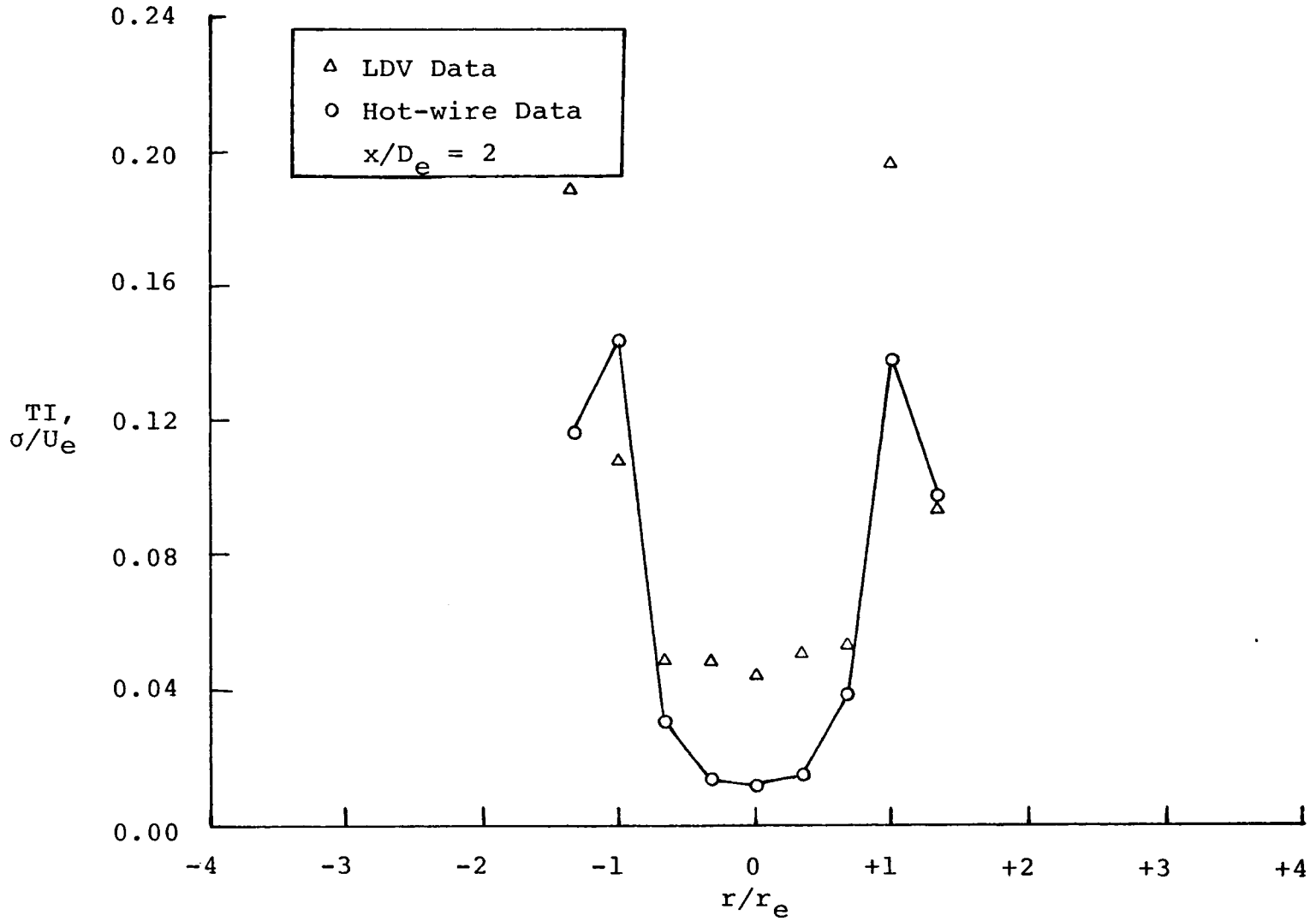



Figure 16. Turbulence intensity measurements at $x/D_e = 2$.

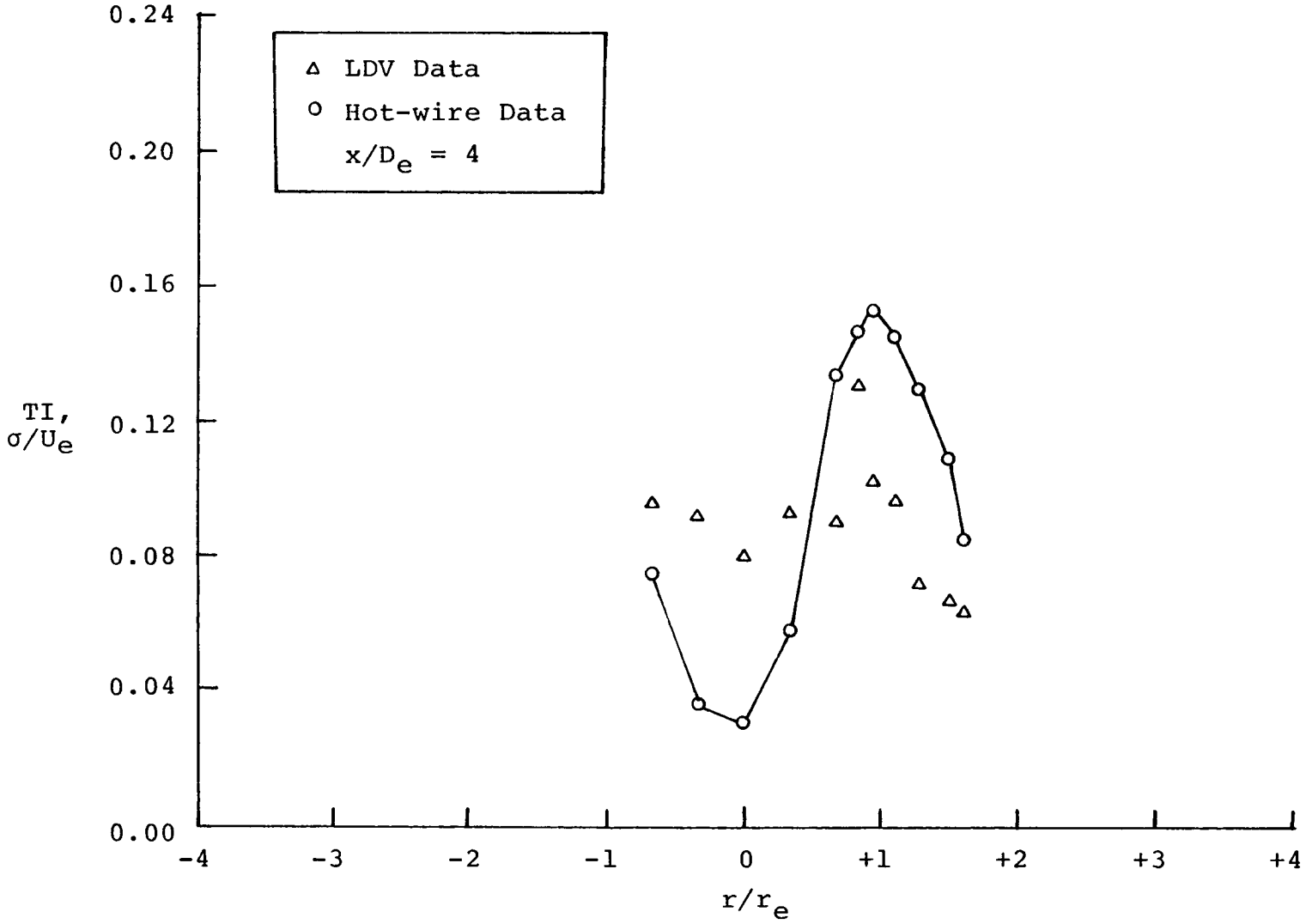



Figure 17. Turbulence intensity measurements at $x/D_e = 4$.

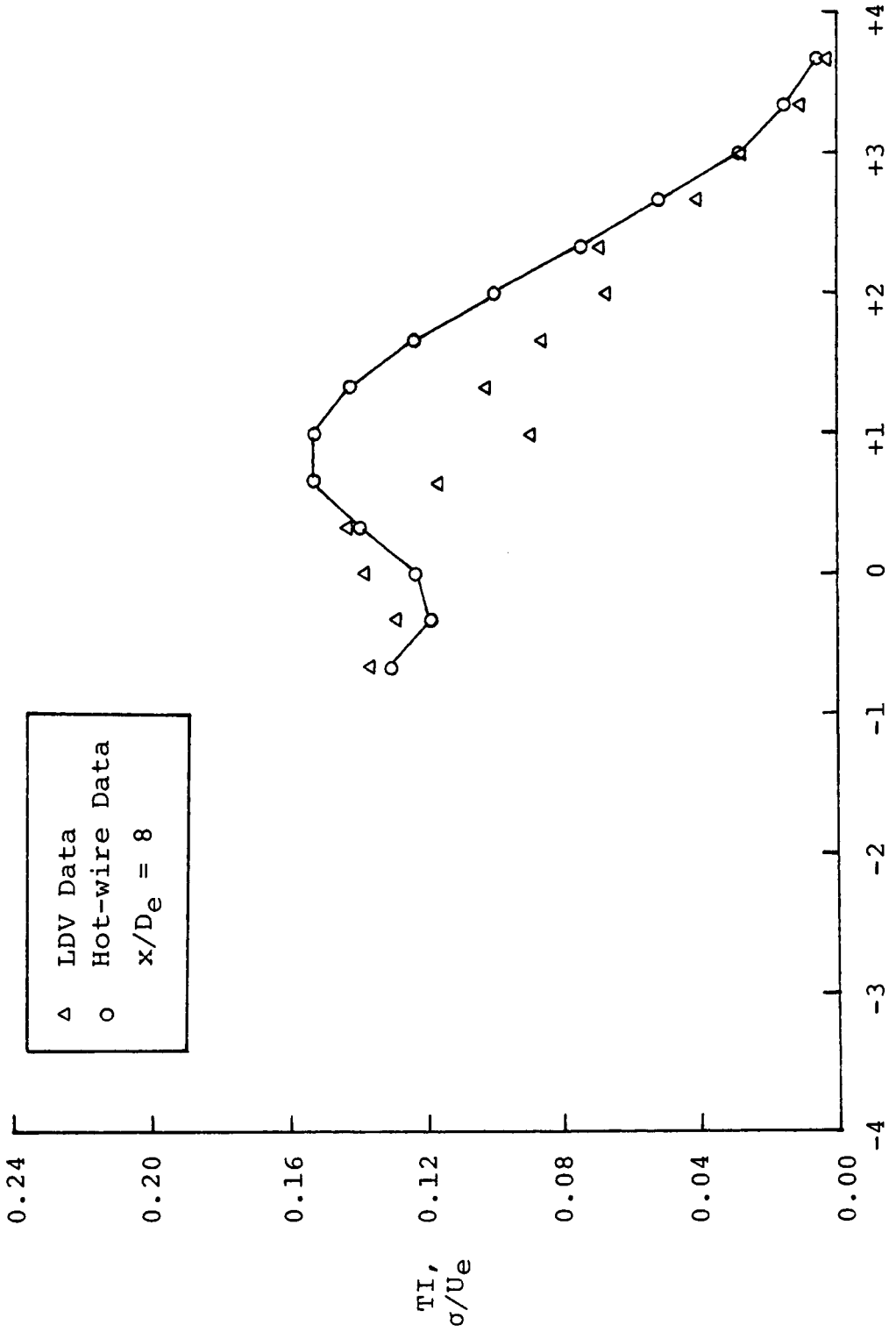



Figure 18. Turbulence intensity measurements at $x/D_e = 8$.

values for the LDV are once again seen to be greater than those for the hot-wire, while in the mixing region the LDV results are less than the hot-wire measurements.

# CHAPTER IV

## DISCUSSION OF RESULTS

The results presented in Chapter III showed some significant differences between the LDV and hot-wire measurements of mean velocity and turbulence intensity in certain regions of the jet flow. These differences are more readily seen if the LDV results are plotted versus the hot-wire measurements. This is done for the mean velocity measurements in Figures 19, 20, 21, and 22 for $x/D_e$ values of 1, 2, 4, and 8, respectively. Similar comparisons for the turbulence intensity results are shown in Figures 23, 24, 25, and 26. The solid line at 45 degrees in these plots corresponds to perfect agreement of the LDV and hot-wire measurements. The broken line indicates a linear least squares curve fit of the data, the equation of which is shown on the plots, along with $R^2$, a correlation coefficient.

An attempt is made in the following sections to interpret the differences seen in the measurements made with the two systems from a qualitative standpoint by considering statistical confidence and bias, geometric alignment, airflow control, particle dynamics, and signal processor parameter effects.

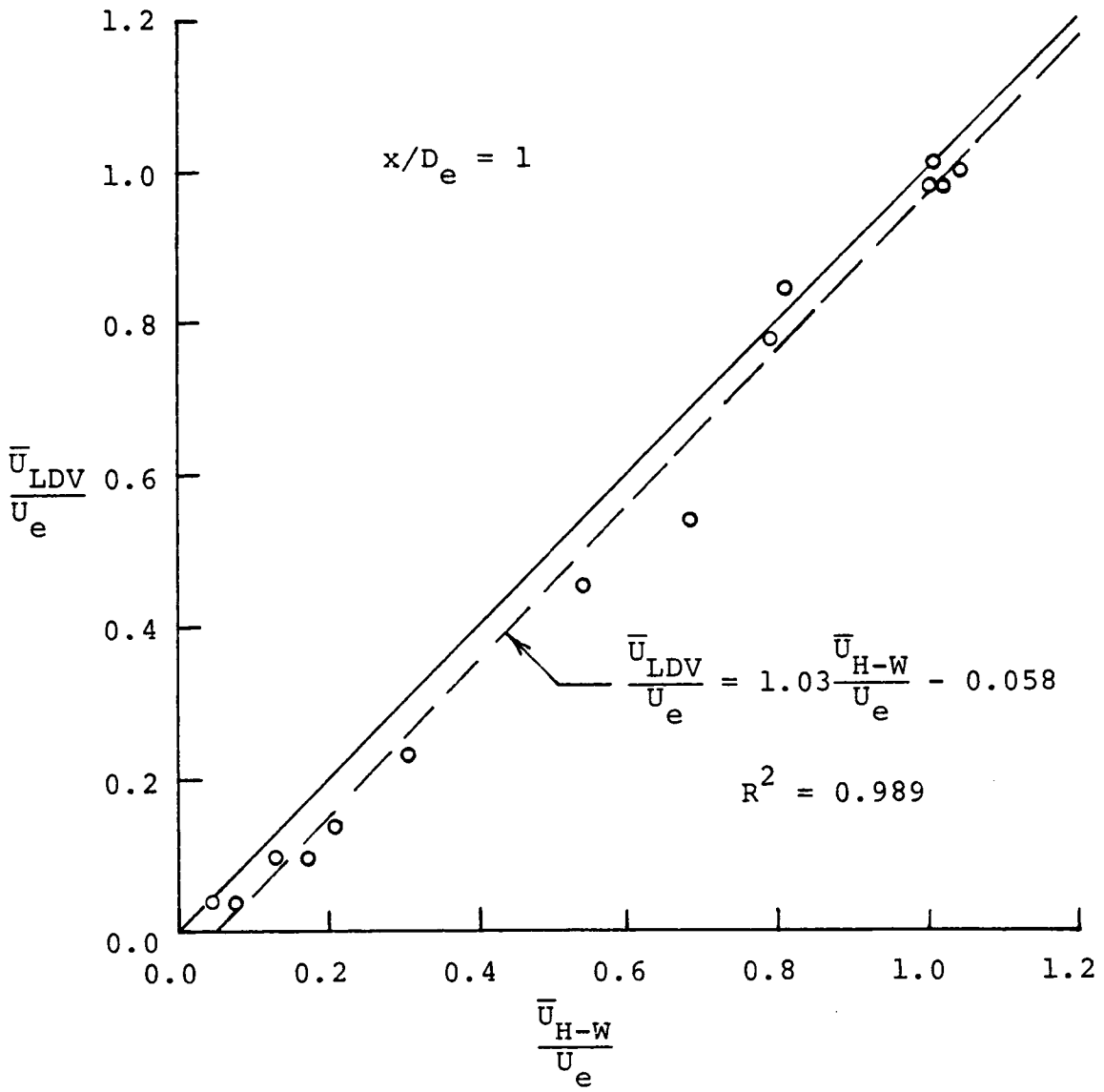



Figure 19. Comparison of LDV and hot-wire measurements of mean velocity at $x/D_e = 1$.

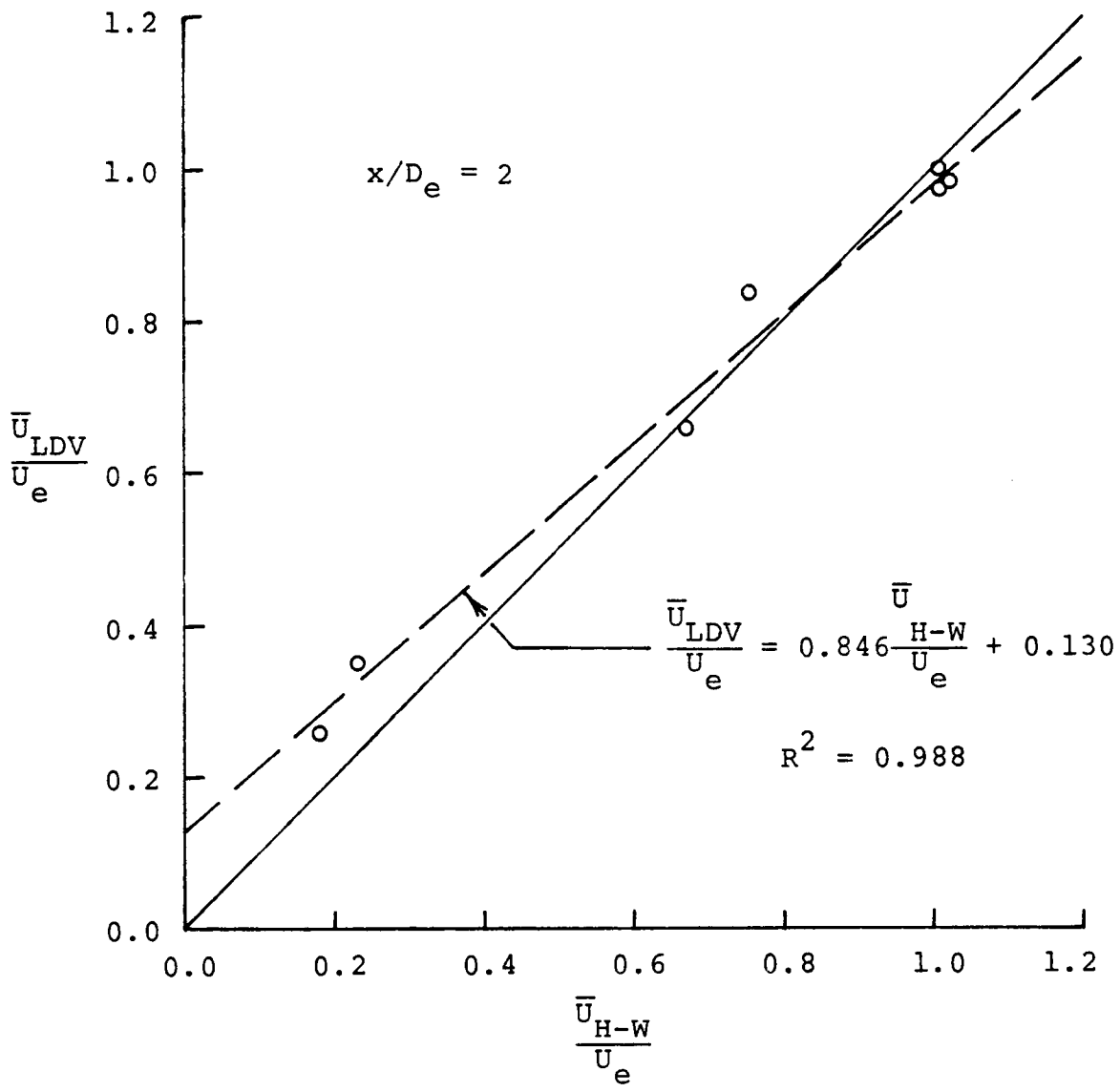



Figure 20. Comparison of LDV and hot-wire measurements of mean velocity at $x/D_e = 2$.

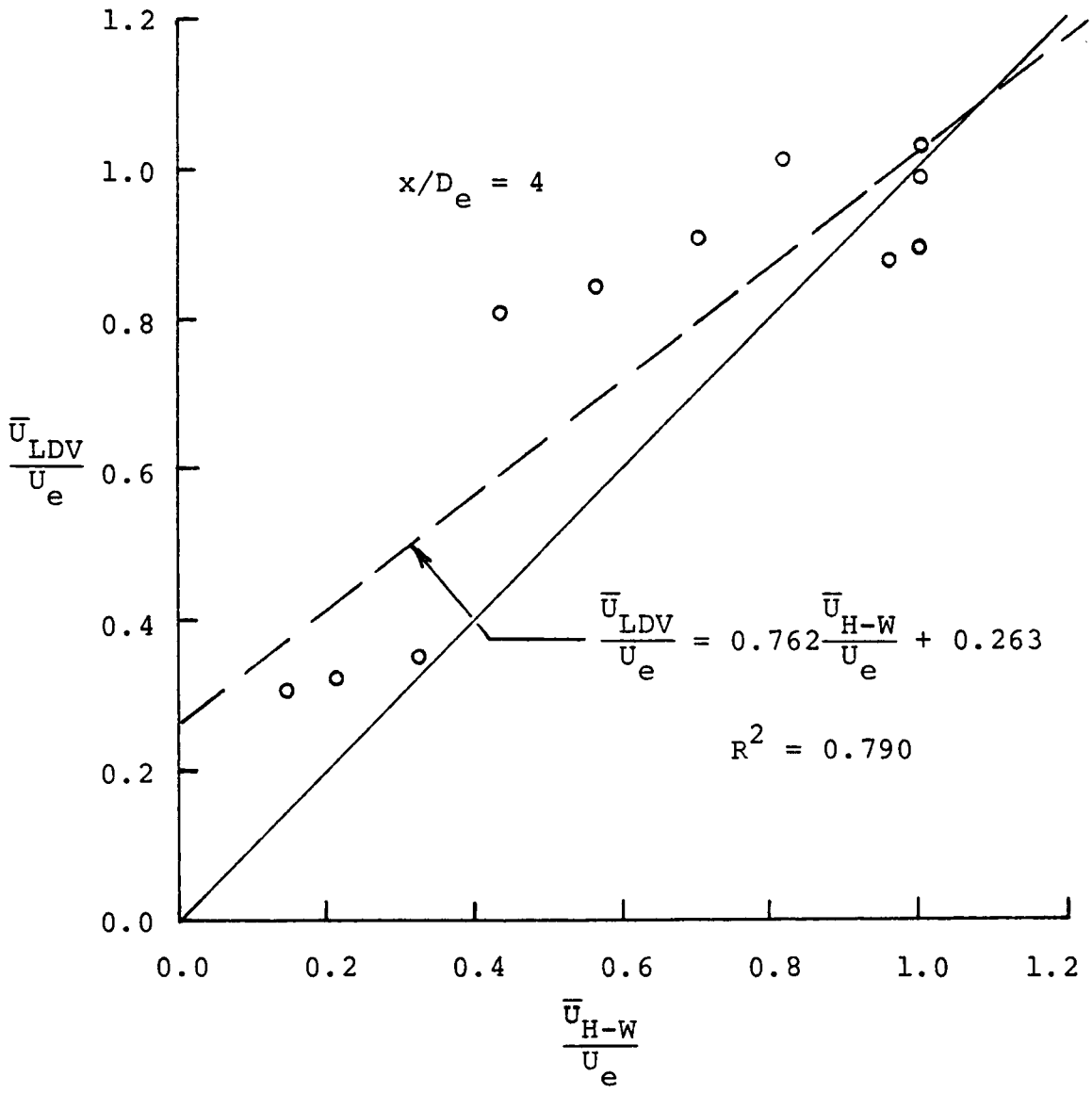



Figure 21. Comparison of LDV and hot-wire measurements of mean velocity at $x/D_e = 4$.

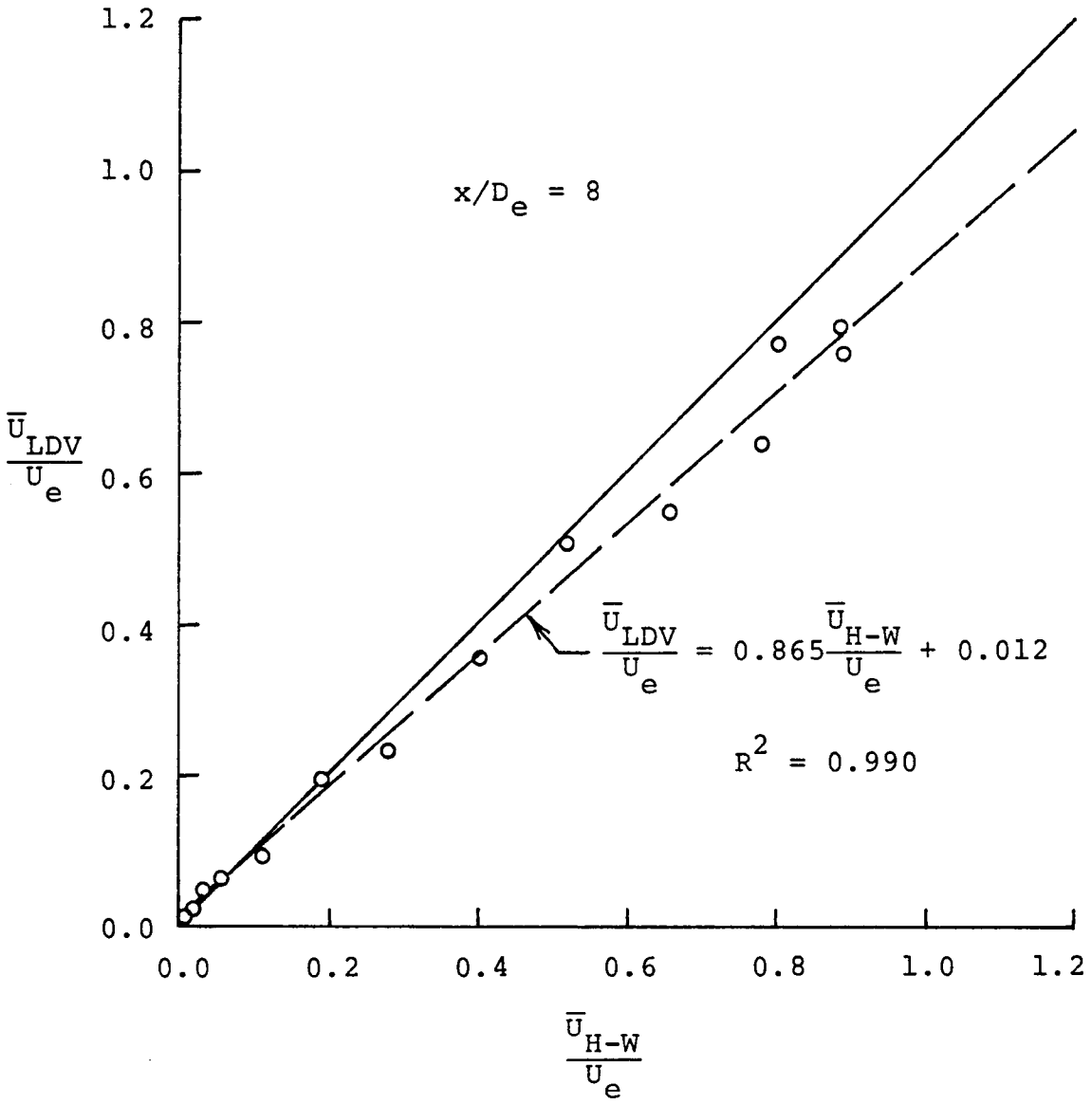



Figure 22. Comparison of LDV and hot-wire measurements of mean velocity at $x/D_e = 8$.

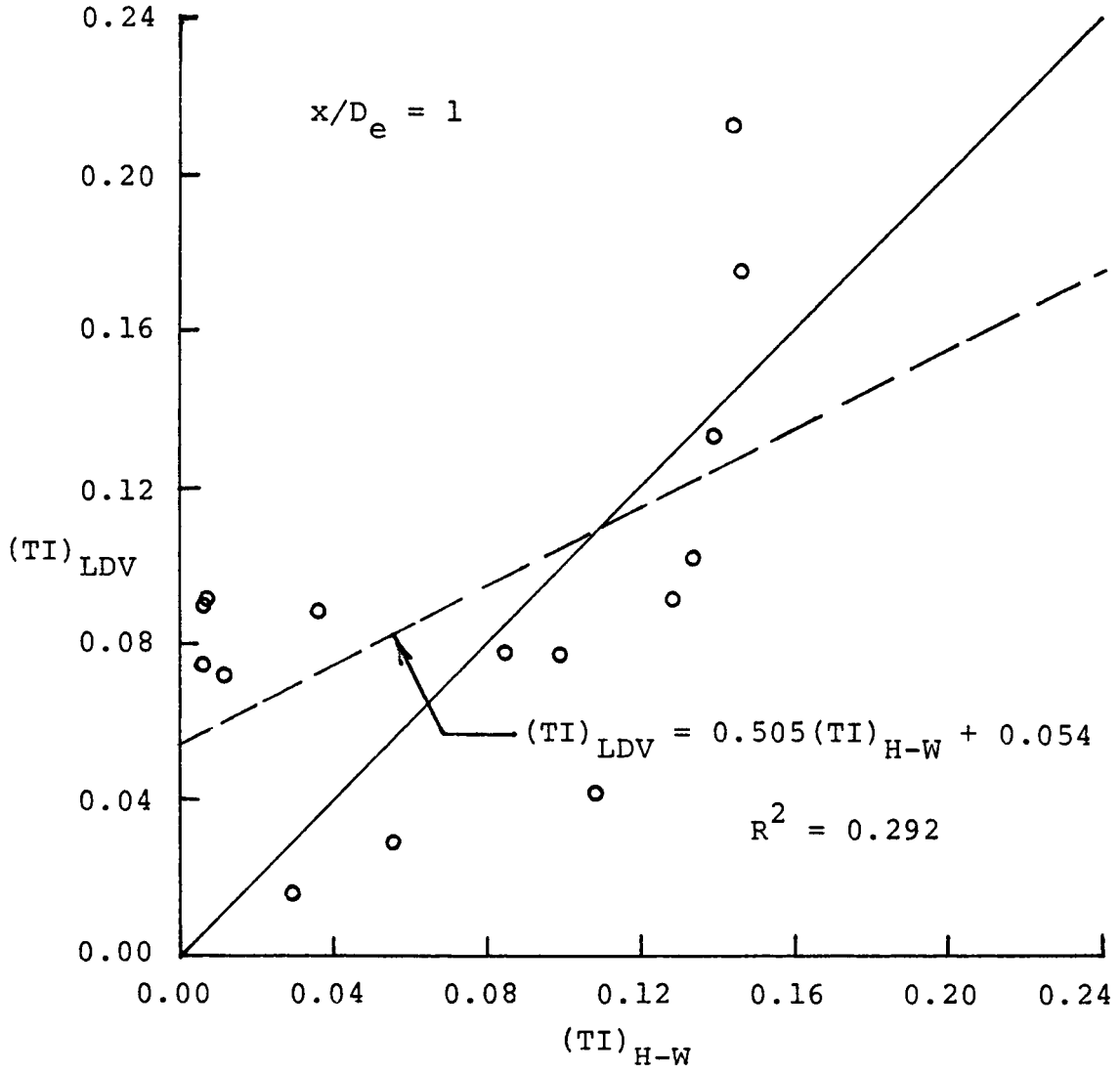



Figure 23. Comparison of LDV and hot-wire measurements of turbulence intensity at $x/D_e = 1$.

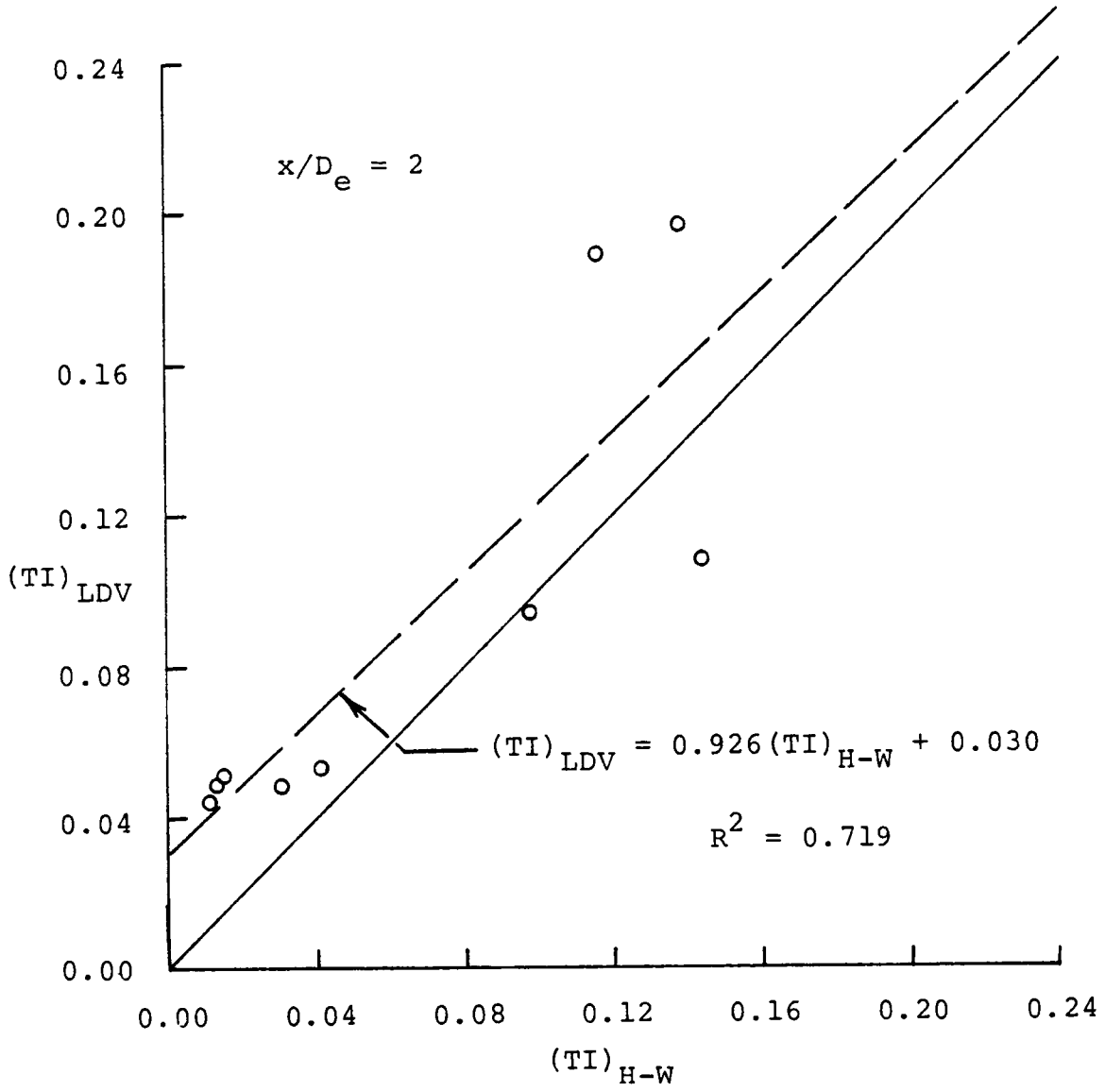



Figure 24. Comparison of LDV and hot-wire measurements of turbulence intensity at $x/D_e = 2$.

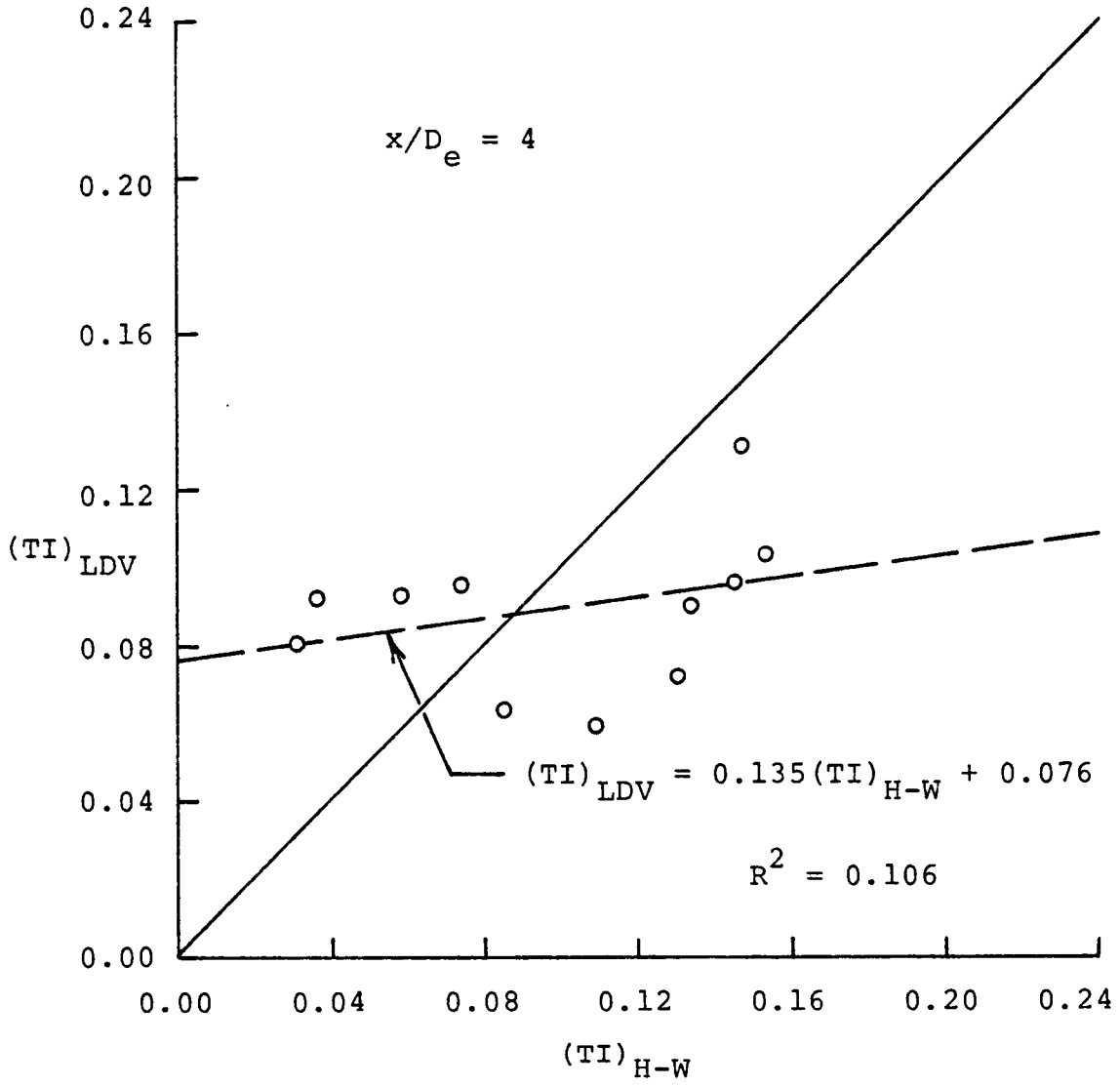



Figure 25. Comparison of LDV and hot-wire measurements of turbulence intensity at $x/D_e = 4$.

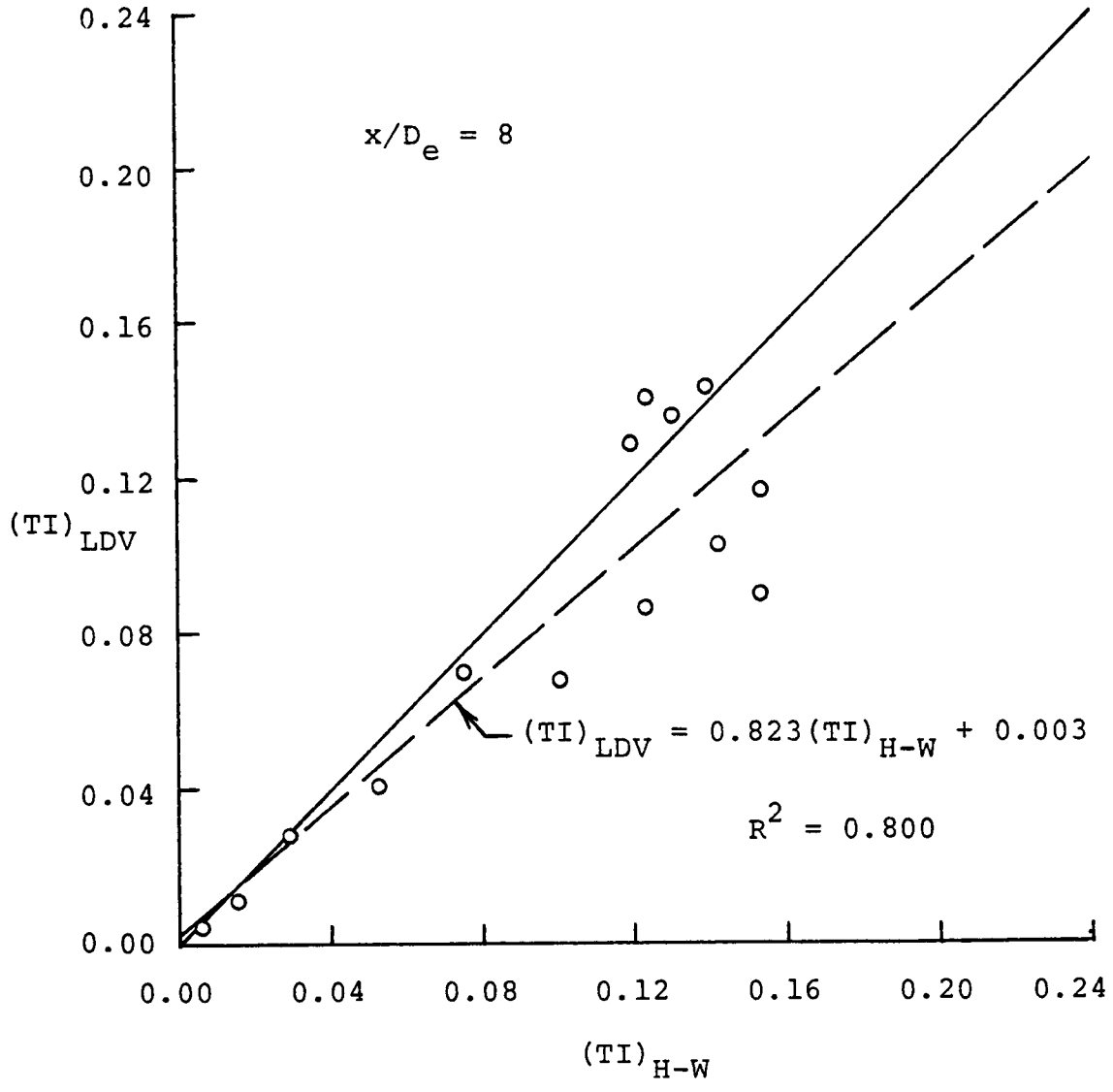



Figure 26. Comparison of LDV and hot-wire measurements of turbulence intensity at $x/D_e = 8$.

## Statistical Considerations

The LDV measurement results are based upon the statistical analysis of a set of individual samples. The accuracy of the results is dependent upon the number of samples in the data set. The number of samples for each data point in this study varied from 30 to 846. Consequently, the accuracy of the measurement results can be expected to vary. An estimate of the tolerance (i.e., the confidence interval) for the mean velocity and turbulence intensity measurements was made using the following approach (3). The tolerance on the local mean velocity measurement, $\overline{U}$, is given by

$$\mathrm{Tol}(\overline{U}) = \frac{Z\ (TI)_{\ell}}{\sqrt{M}} \tag{17}$$

and the tolerance on the local turbulence intensity, $(TI)_{\ell}$, is given by

$$\mathrm{Tol}(TI)_{\ell} = Z\sqrt{\frac{1}{M}\frac{\kappa - 1}{4} + (TI)_{\ell}^{2}} \tag{18}$$

where M is the number of samples in a given set, $\kappa$ is the kurtosis of the set of samples, and Z is the confidence level of the measurement. A value of 2 for Z provides a 95 percent probability that a sample mean is less than two standard deviations from the population mean. It can be seen from Equations 17 and 18 that the tolerance of the mean velocity and turbulence intensity depend upon both the number of samples and the turbulence of the flow.

Calculations of the tolerances for the LDV measurements were made and the results are presented in Tables II, III, IV, and V for $x/D_e$ = 1, 2, 4, and 8, respectively. These tables list the mean velocity, $\bar{U}/U_e$; the local turbulence intensity, $(TI)_\ell$; the kurtosis of the sample set, $\kappa$; the number of samples in the set, M; the digital high pass filter setting used during data collection; the tolerance for the mean velocity, $Tol(\bar{U})$, expressed in percent of the local mean; and the tolerance for the local turbulence intensity, $Tol(TI)_\ell$, expressed in terms of percent of the local turbulence intensity. As expected, the tolerance for the turbulence intensity is seen to be greater for a given number of samples than the tolerance for the mean velocity. Figures 27 and 28 present the tolerances (i.e., confidence intervals) for a 95 percent confidence level for the mean velocity and turbulence intensity at $x/D_e$ = 2, respectively. The intervals for the mean velocity are seen to be rather narrow, while those for the turbulence intensity are broad, particularly in the cases where the local TI is high. This may account for some of the large differences between the LDV and hot-wire results.

The LDV results were calculated from the harmonic mean of a set of individual samples. Such a harmonic average provides an unbiased estimate of the mean fluid velocity if the interval between samples is inversely proportional to the instantaneous velocity of the fluid (6).

TABLE II

LDV DATA ANALYSIS SUMMARY AT $x/D_e = 1$

$\delta = 53.12$ µft
$U_e = 300$ ft/sec

| Test Pt. | $r/r_e$ | $\bar{U}/U_e$ | $(TI)_\ell$ | κ | M | H-P FILTER SETTING | Tol($\bar{U}$) | Tol$(TI)_\ell$ |
|---|---|---|---|---|---|---|---|---|
| 1 | -0.333 | 1.01 | 0.0908 | 2.649 | 339 | 5.0 MHz | 0.986% | 8.75% |
| 2 | 0 | 1.01 | 0.0889 | 2.588 | 324 | 5.0 | 0.988 | 7.07 |
| 3 | 0.333 | 0.978 | 0.0767 | 2.940 | 299 | 5.0 | 0.887 | 8.10 |
| 4 | 0.667 | 0.979 | 0.0734 | 2.807 | 324 | 5.0 | 0.816 | 7.51 |
| 5 | 0.833 | 1.00 | 0.0883 | 2.750 | 310 | 5.0 | 1.00 | 7.58 |
| 6 | 1. | 0.777 | 0.171 | 2.525 | 335 | 3.0 | 1.87 | 7.00 |
| 7 | 1.333 | 0.0399 | 0.400 | 1.998 | 30 | 0.1 | 14.6 | 23.4 |
| 8 | 1.250 | 0.0378 | 0.772 | 3.498 | 45 | 0.05 | 23.0 | 32.9 |
| 9 | 1.208 | 0.0969 | 0.798 | 11.13 | 694 | 0.1 | 6.06 | 13.5 |
| 10 | 1.183 | 0.0947 | 0.812 | 9.844 | 698 | 0.1 | 6.15 | 12.8 |
| 11 | 1.167 | 0.138 | 0.299 | 3.085 | 761 | 0.4 | 2.17 | 5.67 |
| 12 | 1.125 | 0.230 | 0.396 | 5.036 | 846 | 0.5 | 2.72 | 7.42 |
| 13 | 1.083 | 0.455 | 0.385 | 4.178 | 811 | 1.0 | 2.70 | 6.82 |
| 14 | 1.042 | 0.541 | 0.391 | 6.028 | 833 | 1.0 | 2.71 | 8.23 |
| 15 | 0.958 | 0.843 | 0.121 | 2.240 | 184 | 4.0 | 1.78 | 8.40 |

TABLE III

LDV DATA ANALYSIS SUMMARY AT $x/D_e = 2$

$\delta = 65.04$ µft
$U_e = 301$ ft/sec

| Test Pt. | $r/r_e$ | $\bar{U}/U_e$ | $(TI)_\ell$ | κ | M | H-P FILTER SETTING | Tol($\bar{U}$) | Tol$(TI)_\ell$ |
|---|---|---|---|---|---|---|---|---|
| 1 | 0 | 0.973 | 0.0460 | 2.085 | 80 | 4.0 MHz | 1.03% | 11.7% |
| 2 | -0.333 | 0.978 | 0.0504 | 2.410 | 79 | 4.0 | 1.13 | 13.4 |
| 3 | -0.667 | 0.983 | 0.0497 | 2.439 | 84 | 4.0 | 1.08 | 13.1 |
| 4 | -1. | 0.836 | 0.130 | 2.146 | 80 | 3.0 | 2.91 | 12.3 |
| 5 | -1.333 | 0.350 | 0.541 | 9.049 | 694 | 0.1 | 4.11 | 11.5 |
| 6 | 0.333 | 0.981 | 0.0524 | 2.324 | 86 | 4.0 | 1.13 | 12.5 |
| 7 | 0.667 | 0.999 | 0.0533 | 2.697 | 81 | 4.0 | 1.18 | 14.5 |
| 8 | 1. | 0.661 | 0.299 | 8.054 | 84 | 1.0 | 6.52 | 29.7 |
| 9 | 1.333 | 0.256 | 0.368 | 4.195 | 77 | 0.5 | 8.39 | 22.0 |

TABLE IV

LDV DATA ANALYSIS SUMMARY AT $x/D_e = 4$

$\delta = 67.96$ μft
$U_e = 299$ ft/sec

| Test Pt. | $r/r_e$ | $\bar{U}/U_e$ | $(TI)_\ell$ | κ | M | H-P FILTER SETTING | Tol($\bar{U}$) | Tol$(TI)_\ell$ |
|---|---|---|---|---|---|---|---|---|
| 1 | -0.667 | 0.878 | 0.110 | 1.906 | 44 | 3.1 MHz | 3.32 % | 14.7 % |
| 2 | -0.333 | 0.895 | 0.103 | 2.451 | 439 | 3.1 | 0.983 | 5.83 |
| 3 | 0 | 1.03 | 0.0783 | 4.899 | 212 | 3.0 | 1.08 | 13.6 |
| 4 | 0.333 | 0.988 | 0.0941 | 2.786 | 148 | 3.5 | 1.55 | 11.1 |
| 5 | 0.667 | 1.01 | 0.0895 | 3.055 | 211 | 3.5 | 1.23 | 9.95 |
| 6 | 0.833 | 0.908 | 0.145 | 1.998 | 229 | 3.0 | 1.92 | 6.87 |
| 7 | 1. | 0.841 | 0.123 | 1.857 | 217 | 3.0 | 1.67 | 6.50 |
| 8 | 1.167 | 0.807 | 0.120 | 1.994 | 163 | 3.0 | 1.88 | 8.03 |
| 9 | 1.333 | 0.350 | 0.207 | 2.182 | 347 | 1.0 | 2.22 | 6.25 |
| 10 | 1.5 | 0.324 | 0.208 | 1.988 | 298 | 1.0 | 2.41 | 6.24 |
| 11 | 1.667 | 0.306 | 0.207 | 1.674 | 276 | 1.0 | 2.49 | 5.53 |

TABLE V

LDV DATA ANALYSIS SUMMARY AT $x/D_e = 8$

$\delta = 63.72$ μft
$U_e = 299$ ft/sec

| Test Pt. | $r/r_e$ | $\bar{U}/U_e$ | $(TI)_\ell$ | κ | M | H-P FILTER SETTING | Tol($\bar{U}$) | Tol$(TI)_\ell$ |
|---|---|---|---|---|---|---|---|---|
| 1 | -0.667 | 0.770 | 0.177 | 3.544 | 36 | 2.0 $MH_z$ | 5.90% | 27.2 % |
| 2 | -0.333 | 0.792 | 0.163 | 3.273 | 231 | 2.3 | 2.14 | 10.1 |
| 3 | 0 | 0.755 | 0.183 | 2.938 | 259 | 2.3 | 2.27 | 8.94 |
| 4 | 0.333 | 0.639 | 0.224 | 2.913 | 247 | 1.8 | 2.85 | 9.25 |
| 5 | 0.667 | 0.550 | 0.213 | 2.185 | 297 | 1.8 | 2.47 | 6.78 |
| 6 | 1. | 0.507 | 0.178 | 2.172 | 175 | 1.8 | 2.69 | 8.61 |
| 7 | 1.333 | 0.356 | 0.288 | 2.235 | 368 | 1.0 | 3.00 | 6.52 |
| 8 | 1.667 | 0.231 | 0.374 | 3.677 | 458 | 0.5 | 3.50 | 8.41 |
| 9 | 2. | 0.192 | 0.353 | 2.261 | 446 | 0.5 | 3.34 | 6.28 |
| 10 | 2.333 | 0.0935 | 0.746 | 6.442 | 458 | 0.1 | 6.97 | 12.9 |
| 11 | 2.667 | 0.0625 | 0.657 | 2.855 | 385 | 0.1 | 6.70 | 9.65 |
| 12 | 3. | 0.0479 | 0.597 | 1.887 | 414 | 0.1 | 5.87 | 7.47 |
| 13 | 3.333 | 0.0256 | 0.440 | 1.762 | 264 | 0.075 | 5.42 | 7.63 |
| 14 | 3.667 | 0.0156 | 0.282 | 2.733 | 163 | 0.05 | 4.42 | 11.2 |

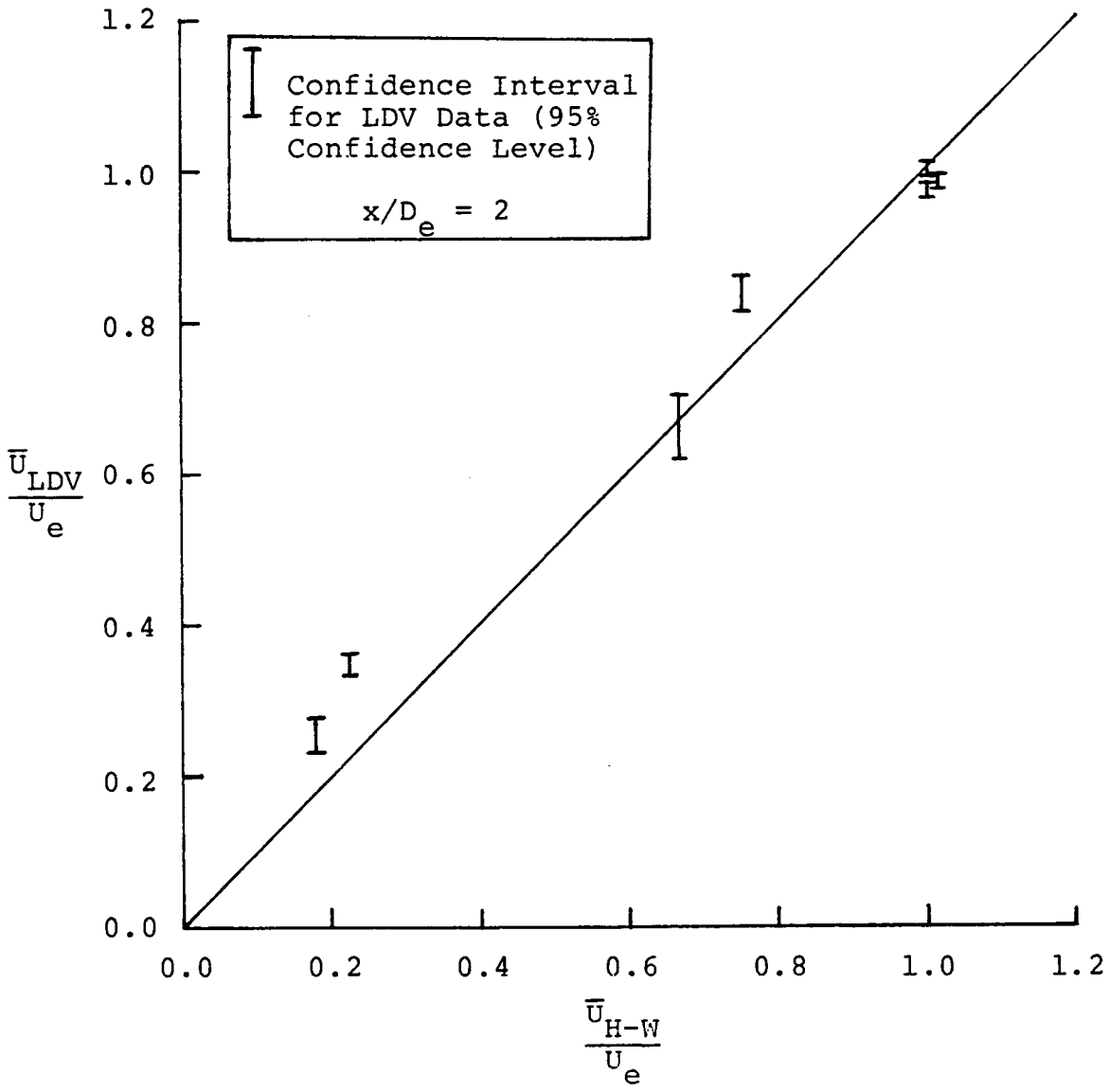



Figure 27. Confidence intervals for LDV mean velocity measurements at $x/D_e = 2$.

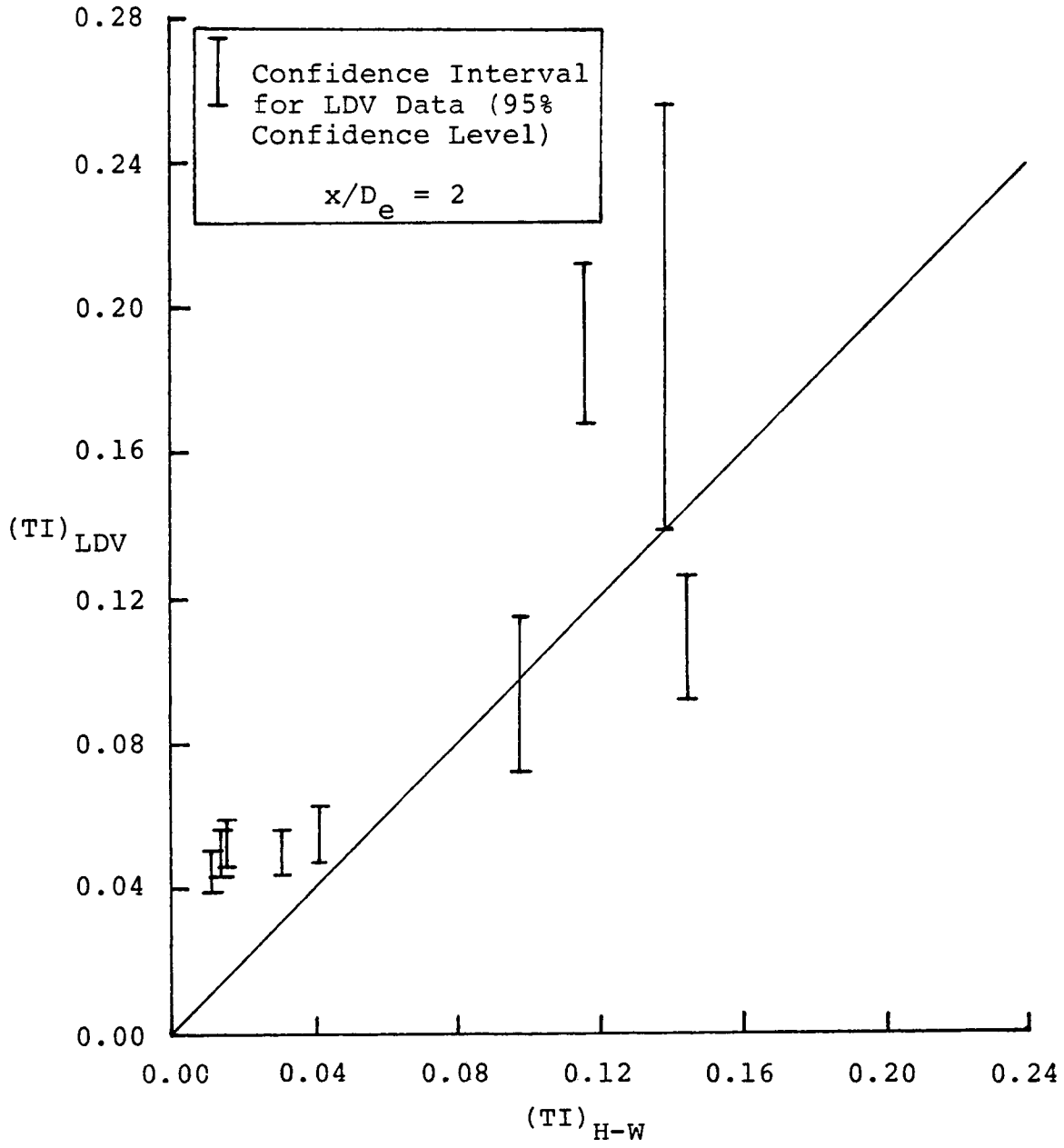



Figure 28. Confidence intervals for LDV turbulence intensity measurements at $x/D_e = 2$.

Then it would be expected that more high velocity particles would traverse the probe volume than slower particles, and an arithmetic mean would be biased toward the higher velocities. This phenomenon is referred to by Flack as individual realization biasing (8). If, however, the sampling process is random, then the arithmetic mean of the individual samples provides the best approximation to the true mean velocity (5). The airflow used in this study was not seeded artificially, so the particle size and concentration are not known specifically. In order to see if an arithmetic average would better fit the LDV data to the hot-wire data, the measurements at $x/D_e = 2$ were recalculated using the arithmetic mean. The results are compared to those for the harmonic mean in Figure 29 for the mean velocity. It may be seen that the arithmetic mean results vary little from those obtained using the harmonic mean calculation.

## Geometric Considerations

Consider the flow to be oriented with respect to the coordinate system shown in Figure 30. Consider also that the LDV probe volume and hot-wire are oriented in the x-z plane as shown. The instantaneous velocity vector may be considered to be composed of a mean velocity, $\overline{U}$, and the fluctuating components u, v, and w along with the x, y, and z axes, respectively. The hot-wire will respond

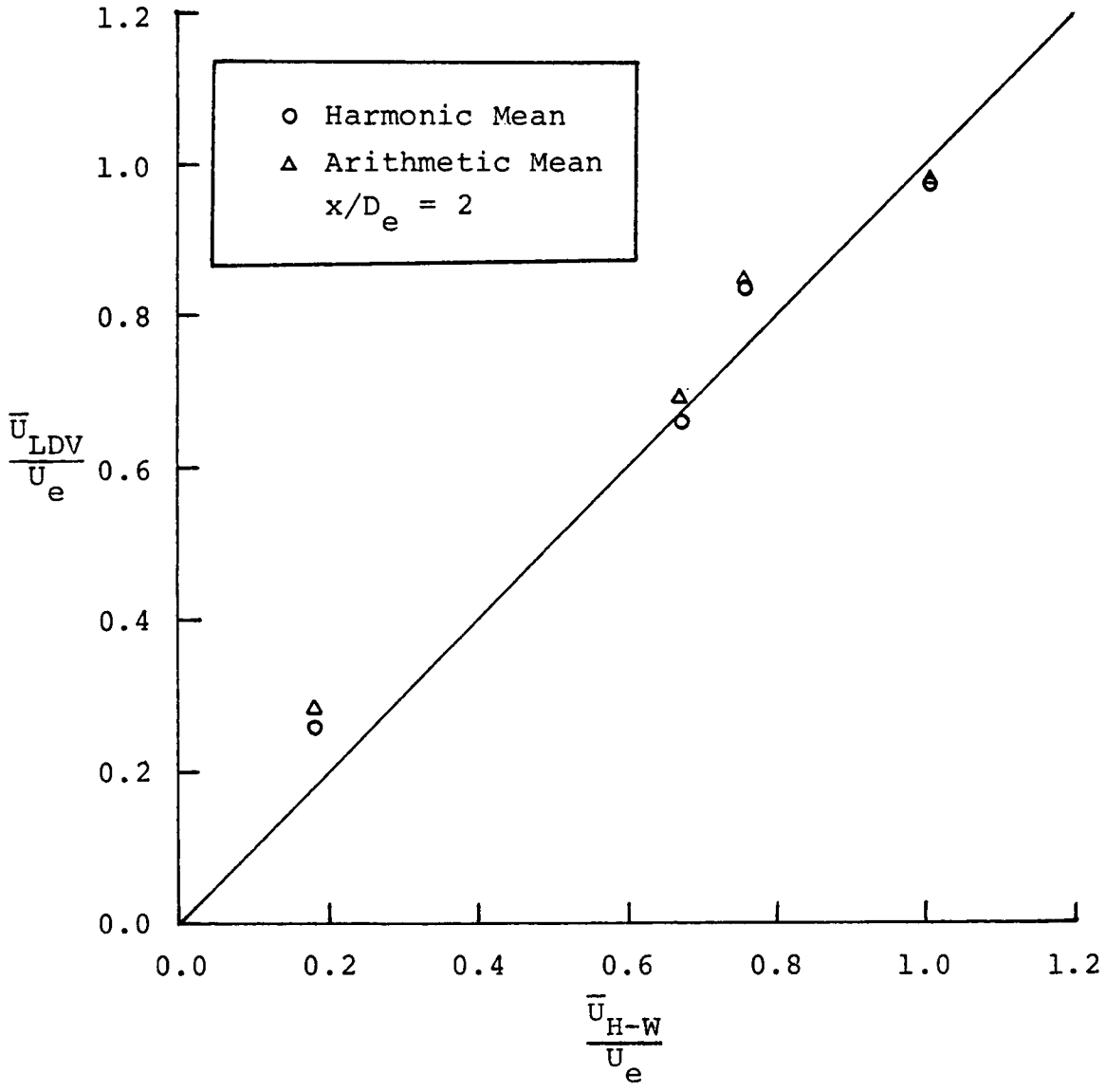
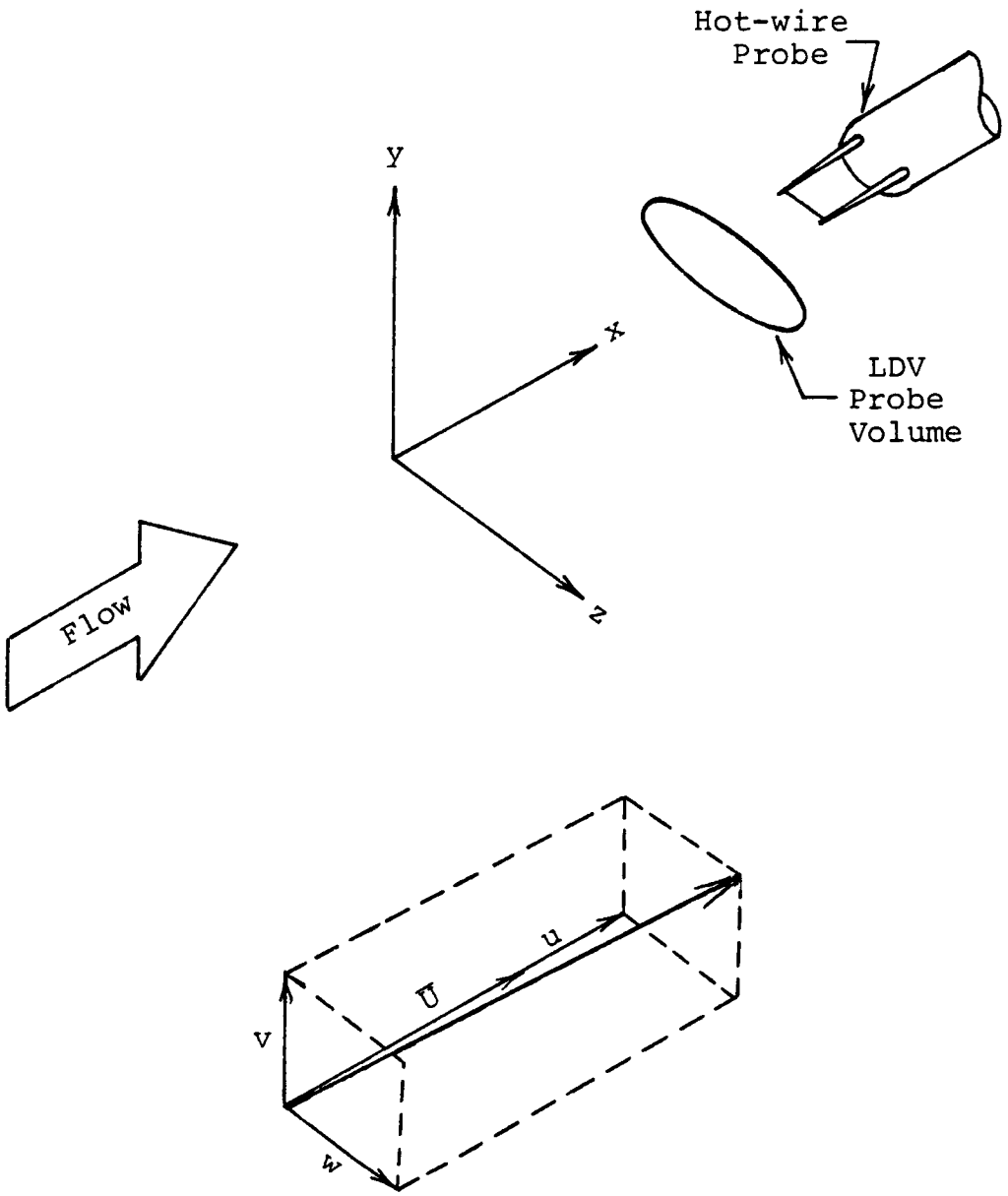



Figure 29. Comparison of LDV results using arithmetic and harmonic means.




$$\text{Instantaneous Velocity} = \sqrt{(\bar{U} + u)^2 + v^2 + w^2}$$

Figure 30. Coordinate system for fluid flow.

primarily to flows in the x and y axes, with the flow along the length of the wire causing little effect. The resulting instantaneous velocity sensed by the hot-wire will be $\sqrt{(\overline{U} + u)^2 + v^2}$. The LDV, on the other hand, responds only to the velocity component which is perpendicular to the interference fringes, i.e., $\overline{U} + u$. In regions of the flow where the turbulence is low, the velocity sensed by the two instruments should be nearly the same. In regions of highly turbulent flow, however, it appears that the hot-wire would indicate a higher mean velocity than the LDV. This trend is not readily apparent in the measurement results, indicating that other factors may be influencing the results more.

Misalignment of the LDV probe volume and the hot-wire probe may also lead to differences in the results obtained with the two systems. Although misalignment in the potential core of the jet should cause litte difference, in the shear layer and mixing region such misalignment could lead to significant anomalies. Figure 14, page 31, indicates that the two probes may not have been aligned during this test run since the LDV data appear shifted with respect to the hot-wire results.

## Airflow Control Considerations

Low frequency oscillations (with a period of several seconds) in the stilling chamber pressure occurred during

testing due to control problems with the globe regulators in the flow line. The airflow in turn varied directly with these pressure oscillations. Since several seconds were required to collect the required number of LDV samples, while the hot-wire data were acquired in much less time, these flow variations could affect the LDV results. The variations in flow would be sensed as velocity oscillations by the LDV and would cause the turbulence intensity seen by the LDV to be greater than that for a non-oscillating flow. This may account for the fact that in the center region of the flow the LDV turbulence intensities were higher than those seen by the hot-wire.

## Particle Dynamics Considerations

As discussed earlier, the LDV measures fluid flow velocity by determining the velocity of particles in the flow. These particles must, therefore, follow the flow accurately if the fluid velocity measurement is to be valid. Large particles may tend to lag the fluid flow. If the velocities of such particles are included in the data set, then the resulting mean velocity and turbulence intensity may be biased. The current LDV signal processor attempted to correct for any such errors with a high pass filter as discussed in the next section.

## Signal Processor Parameter Considerations

The choice of the digital high pass filter cut-off frequency determines the minimum allowable value for a particle velocity in a given sample set. If too high a value is chosen for this limit, then valid data may be rejected and the resulting mean velocity will be biased toward the high end. If, on the other hand, too low a limit is chosen, the velocities of large, slow particles not accurately following the flow may be accepted, thus biasing the flow toward the low end. The effect of using different values for the high pass filter cut-off frequency may be seen in Figure 31 which shows the minimum acceptable velocity for various high pass filter settings. These results may be compared to the high pass filter settings for each data point listed in Tables II, III, IV, and V; pages 49, 50, 51, and 52, respectively.

The signal to noise ratio, S/N, of the LDV signal may be of significance in regions of the flow where the local turbulence intensity is low. Noise included by the system could cause the standard deviation, and therefore the turbulence intensity, of the measured velocities to be higher. This may contribute to the trend seen in the LDV/hot-wire comparisons of TI near the centerline of the jet, where the LDV results are consistantly larger in magnitude than those for the hot-wire.

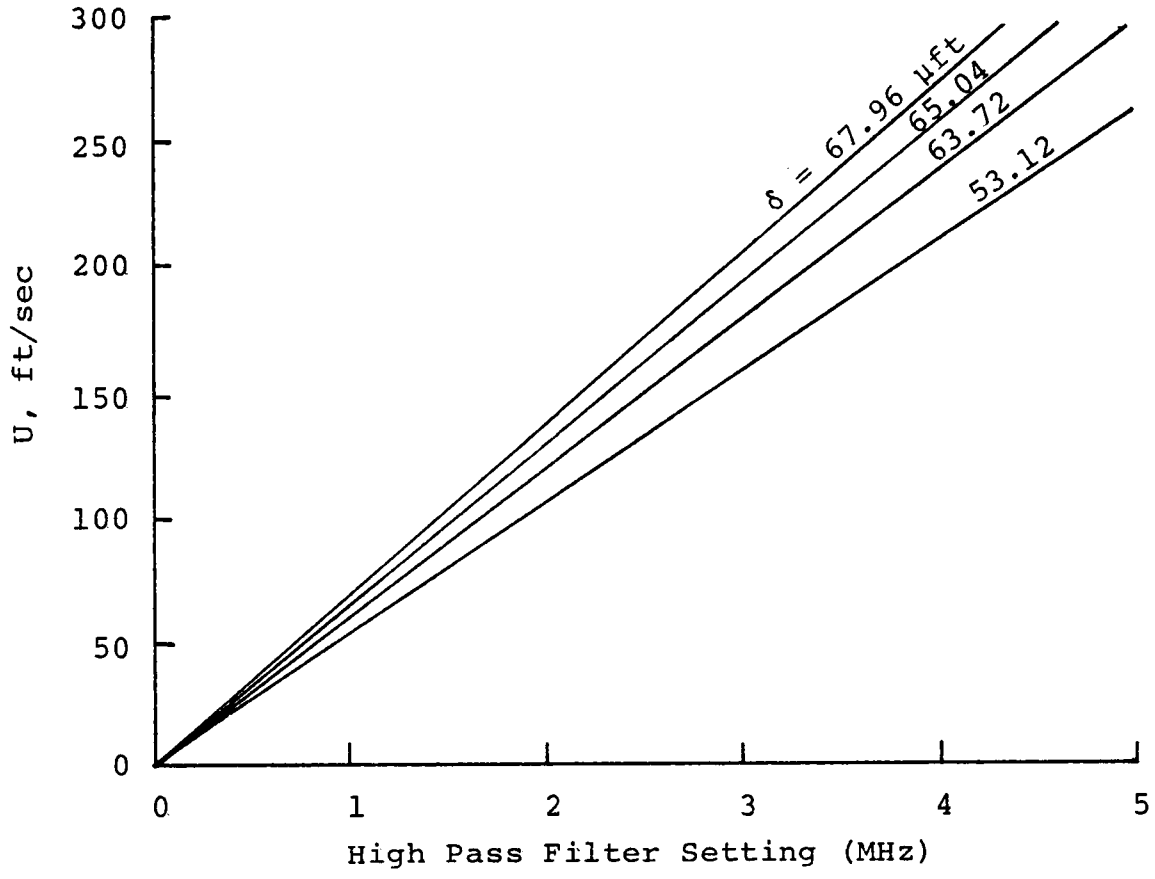



Figure 31. Minimum acceptable velocity for various LDV high pass filter settings.

The aperiodicity limit may also affect the LDV measuremet results. The value used during the current test program was 5 percent. For each test point, a large number of particles were seen to fail this test (see Figure 10, page 26). No comparative measurements were made with a different value for this limit, so no quantitative statement can be made regarding the effect of such a change.

# CHAPTER V

# CONCLUSIONS AND RECOMMENDATIONS

## Conclusions

Measurements of mean velocity and turbulence intensity in an unheated, subsonic, free-jet airflow were made with a single-component, Bragg-diffracted laser Doppler velocimeter. The results were compared with measurements made concurrently with a hot-wire anemometer. The results were obtained for axial locations 1, 2, 4, and 8 nozzle diameters downstream of the nozzle exit plane.

A comparison of the results indicates that, except for one axial location, the mean velocity measurements made by the two systems showed reasonable agreement. Significant anomalies were also noted for the turbulence intensity measurements at all axial locations.

A consideration of the statistical analysis of the LDV results indicates that the confidence intervals for the turbulence intensity measurements are quite broad in regions of the jet where the local turbulence intensity is high. This factor may account for some of the differences seen in the LDV and hot-wire measurements of turbulence intensity. The confidence intervals are broad due to the small sample sizes used in calculating the LDV results.

In regions of the jet which are highly turbulent,

the fact that the LDV responds to only one velocity component while the hot-wire responds to two may affect the results obtained with the two systems, although this was not apparent in the current study. Misalignment of the LDV probe volume and the hot-wire probe may also have contributed to the differences noted in this comparison.

Low frequency airflow oscillations due to control problems may have caused the LDV to indicate a higher turbulence intensity than that seen by the hot-wire near the jet centerline.

Other factors which may have influenced the LDV measurement results include the high pass filter setting, the S/N ratio of the system, particularly in regions of low turbulence, and the aperiodicity test limit.

## Recommendations

Based on the results obtained in the current program, several improvements in the experimental procedure are recommended to provide a better comparison of LDV and hot-wire measurements in turbulent flow field.

1. Obtain a larger number of samples for each LDV data point to improve the statistical confidence of the measurement results.
2. Use a different flow field in which probe misalignment effects would not be as great, such as flow downstream of a screen.

3. Obtain several sets of hot-wire data while collecting the LDV samples to reduce the effects of different sampling intervals.
4. Monitor the airflow carefully and sample the flow only when the proper conditions are achieved to avoid errors due to flow variations.

# BIBLIOGRAPHY

# BIBLIOGRAPHY


1. Instruction and Service Manual for Type 55D01 Anemometer Unit. Denmark. DISA Electronics, 1968.

2. Bradshaw, P. An Introduction to Turbulence and Its Measurement. Oxford: Pergamon Press, Inc., 1975.

3. Cline, V. A. and H. T. Bentley III. "Application of a Dual Beam Laser Velocimeter to Turbulent Flow Measurements," Arnold Engineering Development Center TR-74-56, Arnold Air Force Station, Tennessee, September, 1974.

4. Cliff, William C., et. al., "Simultaneous Comparison of Turbulent Gas Fluctuations by Laser Doppler and Hot Wire," AIAA Journal, 11:748-749, May, 1973.

5. Barnett, D. O. and T. V. Giel, Jr. "Application of a Two-Component Bragg-Diffracted Laser Velocimeter to Turbulence Measurements in a Subsonic Jet," Arnold Engineering Development Center TR-76-36, Arnold Air Force Station, Tennessee, May, 1976.

6. Barnett, D. O. and T. V. Giel, Jr. "Studies of the Statistical Bias and Signal Characteristics of Laser Velocimeters," Arnold Engineering Development Center TR-78-65, Arnold Air Force Station, Tennessee, January, 1980.

7. Giel, Thomas V., Jr. "Studies of Statistical Bias in Turbulent Flow Parameters Measured with a Laser Velocimeter." Ph.D. dissertation, The University of Notre Dame, 1978.

8. Flack, Ronald D., Jr. "The Application of a Laser Doppler Velocimeter (LDV) in Interpreting Turbulent Structure." Ph.D. Thesis, Purdue University, 1975.

9. Brayton, D. B. and W. H. Goethert, "A New Dual-Scatter Laser Doppler-Shift Velocity Measuring Technique," ISA Transactions, 10:40-50, 1981.

10. Morris, Roger D. "Design of a High-Frequency, Programmable, Laser Velocimeter Signal Processor." Unpublished Master's Thesis, The University of Tennessee, Knoxville, 1978.

11. Abernathy, R. B., et. al., Pratt and Whitney Aircraft, and J. W. Thompson, Jr., "Handbook of Uncertainty in Gas Turbine Measurements," Arnold Engineering Development Center TR-73-5, Arnold Air Force Station, Tennessee, February, 1973.

12. Volk, William. Applied Statistics for Engineers. New York: McGraw-Hill Book Company, Inc., 1958.

13. Dean, Robert C., Jr., "Aerodynamic Measurements," Gas Turbine Laboratory, Massachusetts Institute of Technology, Boston: Eagle Enterprises, 1953.

14. Hughes, William F. and John A. Brighton. Schaum's Outline of Theory and Problems of Fluid Dynamics. New York: McGraw-Hill Book Company, Inc., 1967.

# VITA

L. Brent Bates was born in Barnesville, Ohio on July 31, 1955. He attended elementary school in Quaker City, Ohio and was graduated from Zane Trace High School, Old Washington, Ohio, in May 1973. The following fall he entered David Lipscomb College, Nashville, Tennessee, and in June 1977 he received a Bachelor of Science degree in Engineering Science. Following graduation he accepted a graduate research assistantship at the University of Tennessee Space Institute and began study toward a Master's degree.

In December, 1978 he accepted an engineering position with Sverdrup Technology, Inc. (then ARO, Inc.) at the Arnold Engineering Development Center, where he is currently employed.

He received a Master of Science degree in Engineering Science in August, 1983.

The author is a member of the American Institute of Aeronautics and Astronautics.